Article

# Dysregulated RBM24 phosphorylation impairs APOE translation underlying psychological stress-induced cardiovascular disease

He Yang [1,7], Lei Sun [1,7], Xuemei Bai[2,7], Bingcheng Cai[1], Zepeng Tu[1], Chen Fang[2], Yusheng Bian[1], Xiaoyu Zhang[2], Xudong Han[1], Dayin Lv[2], Chi Zhang[2], Bo Li[1], Shaoxiang Luo[3], Bingbing Du[1], Lan Li[1], Yufeng Yao [2], Zhiqiang Dong [1], Zhuowei Huang[4], Guanhua Su[5], Hui Li[2,6] ✉, Qing K. Wang [2] ✉ & Min Zhang [1] ✉

Psychological stress contributes to cardiovascular disease (CVD) and sudden cardiac death, yet its molecular basis remains obscure. RNA binding protein RBM24 plays a critical role in cardiac development, rhythm regulation, and cellular stress. Here, we show that psychological stress activates RBM24 S181 phosphorylation through eIF4E2-GSK3β signaling, which causally links psychological stress to CVD by promoting APOE translation (apolipoprotein E). Using an Rbm24 S181A KI mouse model, we show that impaired S181 phosphorylation leads to cardiac contractile dysfunction, atrial fibrillation, dyslipidemia, reduced muscle strength, behavioral abnormalities, and sudden death under acute and chronic psychological stressors. The impaired S181 phosphorylation of RBM24 inhibits cardiac translation, including APOE translation. Notably, cardiomyocyte-specific expression of APOE rescues cardiac electrophysiological abnormalities and contractile dysfunction, through preventing ROS stress and mitochondrial dysfunction. Moreover, RBM24-S181 phosphorylation acts as a serum marker for chronic stress in human. These results provide a functional link between RBM24 phosphorylation, eIF4E-regulated APOE translation, and psychological-stress-induced CVD.

Stress, including emotional distress, anger, fear, depression, social stress, job strain, or exposure to natural disasters, has long been recognized as a contributing factor in the pathogenesis of CVD, such as coronary artery disease, stroke, stress cardiomyopathy (Takotsubo syndrome), cardiac arrhythmias, and sudden death, independent of traditional risk factors[1–3]. Depending on the duration of the stressor, it is classified as acute or chronic, and is associated with different cardiovascular events. Acute stress is closely related to cardiac rhythm

[1]College of Biomedicine and Health, College of Life science and Technology, Huazhong Agricultural University, Wuhan 430070, China. [2]Center for Human Genome Research, College of Life Science and Technology, Key Laboratory of Molecular Biophysics of the Ministry of Education, Huazhong University of Science and Technology, Wuhan 430074, China. [3]Wuhan Huamei Biotech Co., Ltd, Wuhan 430079, China. [4]Affiliated Wuhan Mental Health Center, Tongji Medical College, Huazhong University of Science and Technology, Wuhan 430010, China. [5]Department of Cardiology, Union Hospital, Tongji Medical College, Huazhong University of Science and Technology, Wuhan 430022, China. [6]School of Biotechnology of Shandong Polytechnic, Jinan, Shandong 250101, China. [7]These authors contributed equally: He Yang, Lei Sun, Xuemei Bai. ✉e-mail: 907055181@qq.com; qingwang118@qq.com; minzhang@mail.hzau.edu.cn

disturbances[4,5], acute myocardial infarction[6], and even sudden cardiac death[7,8]. On the other hand, chronic stress is implicated in the occurrence and aggravation of CVD[9,10]. Several mouse models have been developed to simulate and investigate the impact of psychological stress on overall health. These models include acute stress induced by epinephrine injection, foot shock, and fox urine exposure, as well as chronic stress induced by social isolation or chronic variable stress[11]. While the physiological response to stress is recognized as an effective modulator of cardiovascular health, the underlying molecular mechanisms remain largely unclear.

APOE (apolipoprotein E) is a secreted protein with an important role in lipid metabolism[12]. APOE can interact with the low-density lipoprotein receptor (LDLR), and thereby regulates the processing of triglyceride-rich lipoproteins and cholesterol metabolism[13]. ApoE-deficient ($ApoE^{-/-}$) mice develop hypercholesterolemia and hyperglycemia even when fed with a chow diet, and show atherosclerosis, cardiac hypertrophy, and age-dependent aortic stiffening when fed with a Western diet, and aortic aneurysms when treated with angiotensin II[14,15]. As it is difficult to induce cardiovascular diseases (CVD) in mice, a line of target gene transgenic mice needs to be crossed to $ApoE^{-/-}$ KO mice to examine its impact on CVD[16]. Genomic variants in *APOE* were significantly associated with the risk of Alzheimer's disease and CVD[17,18]. Recent evidence has shed light on the broad roles of APOE beyond lipid metabolism, including serving as a transcriptional factor, modulating cytoplasmic transport, controlling membrane signaling, regulating oxidative stress, inflammatory responses, and mitochondrial function[19,20]. APOE-knockout mice showed marked vascular oxidative stress and significant changes in gene expression related to pathways implicated in redox, inflammation, and endothelial function[21]. Mitochondria are essential for the heart's normal function by providing energy and controlling cardiac rhythm[22]. Dysfunction in mitochondria can impair cardiac excitability by producing an excess of reactive oxygen species (ROS), which affects ion channels and transporters involved in electrical activity. Several studies have linked APOE with mitochondrial function, particularly providing valuable insights into the underlying mechanisms of Alzheimer's disease (AD) and aging. The APOE4 isoform has been specifically linked to impaired mitochondrial function and altered oxidative stress, contributing to the development of Alzheimer's disease and other neurodegenerative diseases[23,24]. Evidence suggests that APOE is present in mitochondria and affects mitochondrial function by regulating the expression of mitochondrial proteins[25]. Furthermore, recent studies have shown that mitochondria profoundly influence Apolipoprotein E expression and secretion[26]. Despite these intriguing findings, further research is crucial to elucidate the impact of APOE on mitochondrial function in relation to cardiac function and electrophysiological activities.

The RBM24 gene encodes RNA-binding motif protein 24, an RNA-binding protein involved in the regulation of alternative splicing of target pre-mRNAs and translation initiation[27,28]. RBM24 is highly expressed in cardiomyocytes and nonmuscle head territories, and its deficiency in mice or zebrafish leads to abnormal development of embryonic hearts, eyes, and inner ears[28–34]. Conditional *Rbm24* knockout (KO) mice at the postnatal stage showed dilated cardiomyopathy (DCM), heart failure, and postnatal lethality[35]. Overexpression of *Rbm24* in adult mouse hearts induced extensive cardiac fibrosis[36]. Therefore, the expression level of *Rbm24* is delicately balanced in the heart as either its KO or overexpression is detrimental to cardiac structure and function. Furthermore, RBM24 ablation in cardiomyocytes leads to a prolonged QT interval due to alteration in $Ca^{2+}$ handling, underscoring its significance in cardiac electrophysiology[37]. Recent studies have uncovered additional physiological roles of RBM24, including its link to altered lipid metabolism, potentially contributing to liver steatosis and chronic inflammation[38]. RBM24 inhibited p53 translation by binding and sequestering eIF4E

(eukaryotic translation initiation factor 4E) on p53 mRNA[28]. On the other hand, *Rbm24* deficiency increased p53 mRNA translation, and the cardiac developmental defect in *Rbm24* null mice was partially rescued by p53 deficiency[28]. RBM24 is a homologous protein of RBM38[28], whereas the serine 195 (S195) phosphorylation of RBM38 was shown to be mediated by GSK3β and modulate translation by interfering with the RBM38-eIF4E interaction[39]. Recently, we identified eIF4E2, an eIF4E homologous protein (4EHP) that functions as an activator of GSK3β to maintain its proline-directed kinase activity, thus regulating the S195 phosphorylation of RBM38[40]. An *Rbm38* S193D knockin (KI) mouse line showed enhanced p53-dependent cellular senescence, a shortened life span, spontaneous tumors, chronic inflammation, and liver steatosis[41]. S195 of RBM38 corresponds to S181 of RBM24, however, the in vivo role of S181 phosphorylation of RBM24 is unknown[28].

It is worth noting that recent studies have revealed that RBM24 is recruited into stress granules (SGs) under various stress conditions[42]. In this study, we aimed to investigate the physiological functions of RBM24 and its phosphorylation under stress conditions by generating an *Rbm24 S181A knockin (KI)* mouse model, where serine 181 was mutated to unphosphorylable alanine. By exposing the *Rbm24 S181A KI* mice to both acute and chronic stressors, we uncovered that RBM24 phosphorylation played a pivotal role in connecting mental stress to the development of CVD.

## Results

### Acute stress reduces muscle strength and induces behavior abnormalities in *Rbm24 S181A KI* mice

To investigate the physiological role of the S181 phosphorylation of RBM24, we developed an *Rbm24 S181A knockin (KI)* mouse model with the key phosphorylation site at serine−181 mutated to alanine (Supplementary Fig. 1a, b). Compared with wild-type (WT) littermates, *S181A KI* mice showed a normal expression level of RBM24, but no S181 phosphorylation (Supplementary Fig. 1c). *S181A KI* mice were born at a normal Mendelian ratio and grew and developed normally. Histological analysis did not detect obvious pathological abnormalities in *S181A KI* hearts (Supplementary Fig. 1d).

To investigate the potential role of RBM24 phosphorylation under stress conditions, we induced physiological effects of acute stress in mice through intraperitoneal injection of epinephrine. Following epinephrine injection, *S181A KI* mice were rapidly paralyzed, and their maximal or average limb grip strength was significantly reduced compared with WT mice (Fig. 1a, b).

TMT (2,5-dihydro-2,4,5-trimethylthiazoline, a component of fox feces) induces innate fear of the predator odor, and causes acute stress to mice[43]. Under TMT exposure, WT mice exhibited the "freezing" behavior with shorter trajectories in the open field, but still made strenuous movements, such as jumping, to avoid danger or express fear. Strikingly, TMT induced complete freezing of *S181A KI* mice as reflected in the drastic shortening of their trajectories in open fields (Fig. 1c).

### Acute stress induces cardiac electrophysiological abnormalities in *S181A KI* mice

Given the atypical response of *Rbm24 S181A KI* mice to acute stress and the high expression of RBM24 in cardiomyocytes, we hypothesized that RBM24 phosphorylation linked psychological stress to cardiac health. To test this hypothesis, we recorded electrocardiograms (ECGs) from mice injected with 1 mg/kg epinephrine intraperitoneally for three consecutive days to induce acute stress. *S181A KI A/A* mice showed significantly reduced P wave amplitude with or without epinephrine treatment compared with WT mice (Table 1). QTc was significantly shortened in *S181A KI A/A* mice under stress (Table 1). No significant difference was observed in other ECG parameters (Table 1). The most interesting finding was that epinephrine administration was associated with atrial fibrillation (AF, irregular RR intervals with
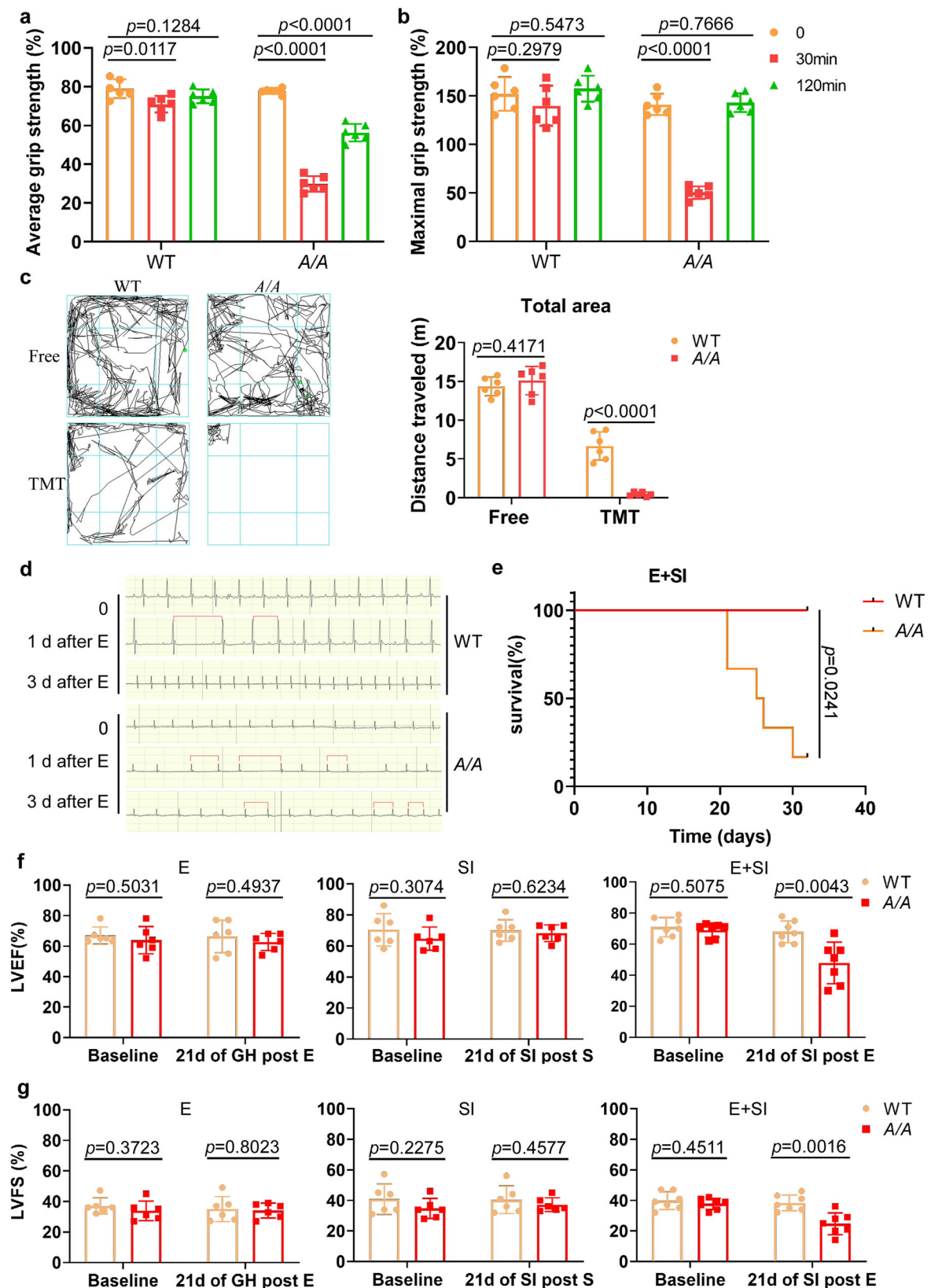
absence of P waves), the most common cardiac arrhythmia in a clinical setting, in *S181A KI A/A* mice, whereas WT mice showed only sinus arrhythmias (irregular RR intervals with the presence of P waves) (Fig. 1d). Our data show that disruption of the S181 phosphorylation of RBM24 causes electrophysiological abnormalities, including reduced P wave amplitude, shortened QTc, and AF under acute stress.

**Stress induces cardiac contractile dysfunction in *S181A KI* mice**

Social isolation (SI), as a chronic stressor, is a particularly malignant bio-behavioral risk factor for the development of cardiovascular diseases. We found that chronic stress of SI for 30 days did not cause apparent behavior abnormalities or cardiac abnormalities in *S181A KI* mice (Supplementary Fig. 1e). However, SI for 30 days in combination

**Fig. 1 | Acute stress reduces muscle strength and induces behavior and cardiac abnormalities in *Rbm24 S181A KI* mice. a, b** Epinephrine decreased average and maximum grip strength in *S181A KI* mice. WT and *A/A* mice were injected intraperitoneally with epinephrine (E, 5 mg/kg), and then the average (**a**) and maximum (**b**) grip strength were recorded at 0, 30, or 120 min (*n* = 6), two-way analysis of variance ANOVA with Bonferroni post hoc correction for multiple comparisons. **c** TMT reduced open field activity of *A/A* mice. The total distance traveled (m) within 3 min was measured in the open field test before and after TMT exposure. Typical locomotion tracks in open-field tests were shown at the left, and quantification of the distance traveled in the total area was shown at the right (*n* = 6), two-way ANOVA with Bonferroni post hoc correction for multiple comparisons.

**d** Detection of AF by ECG recordings of mice 1 day (D) or 3 days after E injection (1 mg/kg, once daily) as compared with mice before E injection. **e** E + SI led to the death of *A/A* mice. WT and *A/A* mice were injected with a single dose of E (2 mg/kg) intraperitoneally and subjected to social isolation (SI). The survival rate of mice was recorded (*n* = 10), log-rank Mantel-Cox test. **f, g** Echocardiographic analysis of left ventricular ejection fraction (LVEF) (**f**) and left ventricular fractional shortening (LVFS) (**g**) at baseline, 21 days of GH (group housing) post E, 21 days of SI post-S (saline), and 21 days of SI post E (E, *n* = 6; SI, *n* = 6; E + SI, *n* = 7), two-way ANOVA with Bonferroni post hoc correction for multiple comparisons. Data were shown as mean ± SD (**a, b, c, f, g**) from six to seven independent experiments.

## Table 1 | ECG characteristics from mice treated with continuous epinephrine injection

|  | WT (*n* = 6) |  |  | *Rbm24 S181 A/A* (*n* = 6) |  |  |
|---|---|---|---|---|---|---|
| Time (Days) | 0 | 1 | 3 | 0 | 1 | 3 |
| HR (bpm) | 536 ± 76 | 416 ± 83 | 466 ± 79 | 437 ± 44 | 427 ± 85 | 404 ± 49 |
| PR (msec) | 36.4 ± 3.2 | 36.7 ± 4.4 | 36.5 ± 2.4 | 37.6 ± 0.8 | 37.7 ± 2.4 | 41.0 ± 3.5 |
| QT (msec) | 37.4 ± 2.5 | 40.6 ± 2.0 | 35.3 ± 1.5 | 30.3 ± 1.1*** | 30.3 ± 2.4*** | 26.3 ± 3.2*** |
| QTc | 35.9 ± 2.9 | 33.1 ± 3.4 | 30.7 ± 3.8 | 28.3 ± 2.9** | 24.6 ± 2.2*** | 22.1 ± 3.3** |
| QRS (msec) | 22.7 ± 3.1 | 24.9 ± 2.3 | 20.2 ± 1.6 | 18.4 ± 1.5 | 21.7 ± 1.4 | 22.2 ± 1.7 |
| AmpP (mv) | 0.16 ± 0.03 | 0.12 ± 0.04 | 0.11 ± 0.04 | 0.08 ± 0.02*** | 0.03 ± 0.01*** | 0.02 ± 0.01*** |
| AmpQ (mv) | −0 ± 0.02 | −0 ± 0.01 | −0 ± 0.01 | −0 ± 0.01 | −0 ± 0.01 | −0 ± 0.01 |
| AmpR (mv) | 1.09 ± 0.06 | 1.15 ± 0.16 | 1.02 ± 0.07 | 0.90 ± 0.19 | 0.90 ± 0.25 | 0.88 ± 0.09 |
| AmpS (mv) | −0.38 ± 0.05 | −0.38 ± 0.04 | −0.37 ± 0.04 | −0.26 ± 0.12 | −0.11 ± 0.22 | −0.20 ± 0.09 |

The *P* value was determined by a two-tailed unpaired Student's *t*-test.

*HR* heart rate, *PR* PR interval, *QT* QT interval, *QTc* QT interval corrected for HR, *QRS* QRS interval, *AmpP* amplitude of P wave, *AmpQ* amplitude of Q wave, *AmpS* amplitude of S wave.

*$p < 0.05$; **$p < 0.01$; ***$p < 0.001$.

with acute stress with injection of a reduced amount of 2 mg/kg epinephrine caused death in *S181A KI* mice starting at 21 days after injection (Fig. 1e). The Kaplan–Meier survival analysis showed that the survival rate of *S181A KI* mice was dramatically reduced compared with WT mice under stress (Fig. 1e).

Echocardiography was used to assess the effect of stress on cardiac structure and function. Echocardiography did not identify any significant effect by stress with 7-day SI and epinephrine injection in *S181A KI* mice (Supplementary Fig. 1f, g). However, at the same time point as the starting time of death, i.e., 21-day SI after epinephrine injection, *S181A KI* mice showed significantly reduced left ventricular ejection fraction (LVEF%) and left ventricular fraction shortening (LVFS %) compared with WT mice (Fig. 1f, g). To assess stress exposure in both genotypes, we measured the serum levels of epinephrine (E) and norepinephrine (NE) at 21 days post-SI following E injection, and found a similar increase in E and NE levels in both *A/A* and WT mice (Supplementary Fig. 1h). Together, these data suggest that acute stress in combination with longer time chronic stress induces cardiac contractile dysfunction and death in *S181A KI* mice.

### Stress damages cardiomyocyte membranes and induces cardiac fibrosis in *S181A KI* mice

Troponin I (Tn-I) is a biomarker for cardiomyocyte damage with high sensitivity and specificity[44]. Serum Tn-I levels were measured after epinephrine injection for 4 consecutive days (1 mg/kg, once daily), and found to be significantly increased in *S181A KI A/A* mice compared with WT mice (Fig. 2a). The data suggest that acute stress damages cardiomyocyte membranes of *A/A* mice. The conclusion was further validated by cardiac permeability assays with Evans blue dye. Acute stress with epinephrine injection for 4 consecutive days induced dramatic increases in cardiac permeability in *S181A KI A/A* mice compared with WT mice (Fig. 2b). Furthermore, repeated TMT exposure (once per day for 7 days) induced elevated serum Tn-I levels and Evans blue dye staining in *A/A* mice, but not in WT mice (Supplementary Fig. 2a, b). In

addition, multicolor immunofluorescence analysis checking different markers showed increased Tn-I staining in *A/A* hearts, indicating cardiomyocyte necrosis, following acute exposure to epinephrine, whereas no such effect was observed in WT hearts (Supplementary Fig. 2c). Together, these data indicate that acute stress induces cardiomyocyte membrane damage in *S181A KI* mice, which may be a key mechanism for abnormal cardiac electrophysiological and contractile functions observed in these mice.

Cardiac fibrosis is a major cause of cardiac contractile dysfunction and AF, and Masson's trichrome staining showed that combined epinephrine treatment and SI (E + SI) induced dramatic cardiac fibrosis in *S181A KI A/A* mice compared with WT mice with E + SI treatment or *A/A* and WT mice treated with SI or E alone (Fig. 2c). Moreover, long-term SI (1 year), without the initial E injection, induced cardiac fibrosis in *S181A KI A/A* mice compared with those in group housing (GH) (Fig. 2d). Chronic variable stress (CVS) also induced dramatic cardiac fibrosis in *S181A KI A/A* mice within one month compared with WT mice (Supplementary Fig. 2d). Taken together, these data indicate that stress induces cardiac fibrosis in *S181A KI* mice (but not in WT mice), a key to abnormal cardiac electrophysiological and contractile functions observed in these mice.

### Impaired translation of APOE in *S181A KI* mice cardiomyocyte

To identify the molecular mechanism for the cardiovascular phenotypes detected in *S181A KI* mice, we took advantage of Pep8, a short peptide disrupting RBM38-eIF4E interaction by targeting eIF4E-binding domain of RBM38 and activating RBM38-mediated translation[45]. GST-RBM24 pull-down assays showed that Pep8 also inhibited the interaction between RBM24 and eIF4E (Supplementary Fig. 3a), and Tat-Pep8 (Pep8 fused with HIV-1 Tat-derived cell-penetrating peptide) increased p53 expression in H9C2 cardiac cells (Supplementary Fig. 3b). L-azidohomoalaine (AHA) labeling assays showed that the level of newly synthesized p53 (translation) was increased by knockdown of RBM24 (Supplementary Fig. 3c) or Tat-Pep8 treatment of H9C2 cells
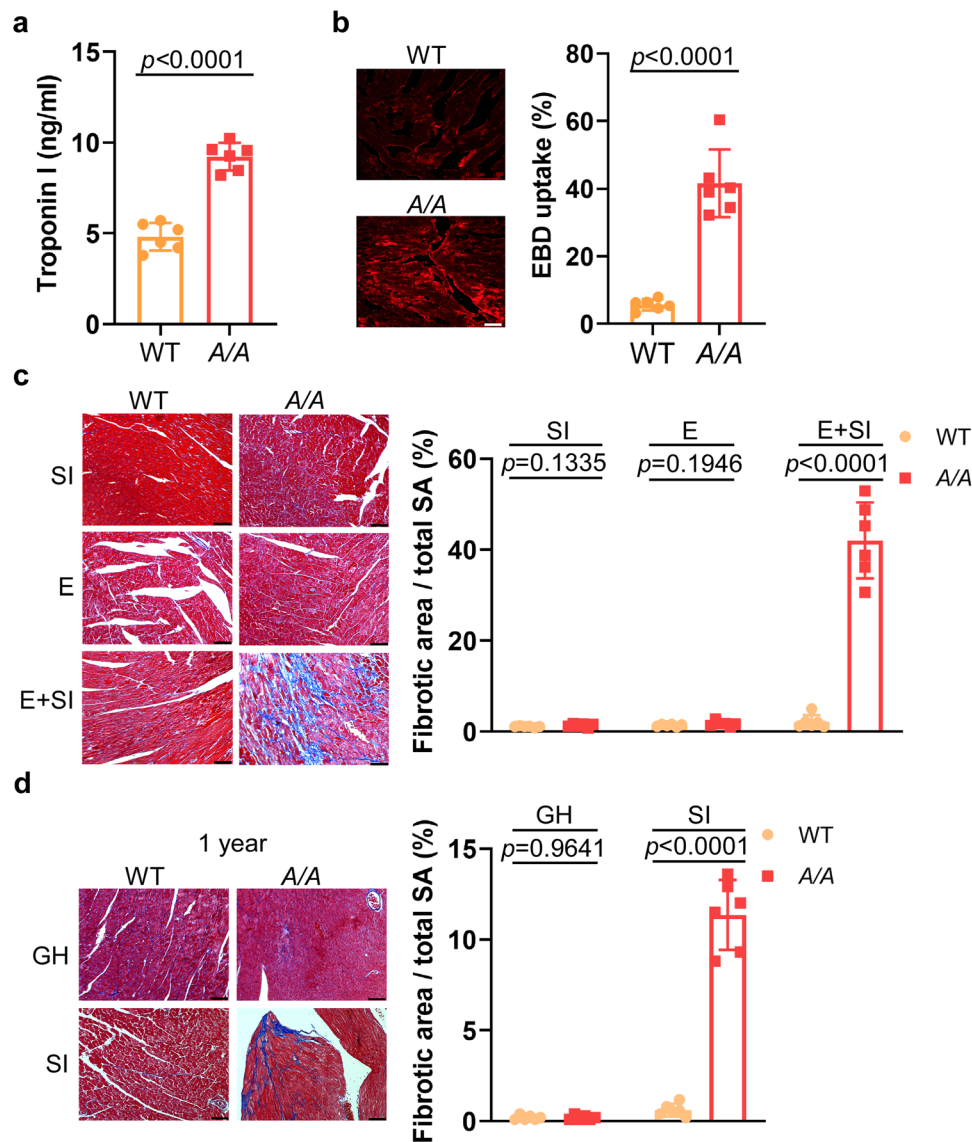
**Fig. 2 | Stress induces cardiomyocyte membrane damage and cardiac fibrosis in *S181A KI* mice. a** Continuous injection of epinephrine (E) increased Tn-I levels in *A/A* mice compared to WT mice. The serum troponin I (Tn-I) levels were measured in mice after 4 consecutive days E injection (1 mg/kg, once daily) (*n* = 6), two-tailed unpaired Student's *t*-test. **b** Continuous injection of E caused cardiomyocyte damage in *A/A* mice. Representative images were shown for Evans blue dye (EBD) uptake in cardiomyocytes of mice after 4 consecutive days of epinephrine injection (1 mg/kg, once daily) at the left, and quantification of the damaged area indicated by EBD was shown at the right (*n* = 6). Scale bars, 50 μm, two-tailed unpaired Student's *t*-test. **c** Combined treatment of SI and E induced cardiac fibrosis in *A/A* mice.

Representative images of Masson's trichrome-stained heart sections were shown at the left and quantification of the fibrosis area was shown at the right (*n* = 6). Scale bars, 50 μm, two-way ANOVA with Bonferroni post hoc correction for multiple comparisons. **d** Long-term SI induced cardiac fibrosis in *A/A* mice. WT and *A/A* mice were housed in SI or GH for 1 year (without initial E injection). Representative images of Masson's trichrome-stained heart sections were shown at the left and quantification of the fibrosis area was shown at the right (*n* = 6). Scale bars, 50 μm, two-way ANOVA with Bonferroni post hoc correction for multiple comparisons. All data were shown as mean ± SD from six independent experiments.

(Supplementary Fig. 3d). The data suggest that Pep8 disrupts RBM42-eIF4E interaction and knockdown of RBM24 increase p53 expression, probably by releasing eIF4E from the RBM42-eIF4E complex, and thereby activating the translation of p53.

Western blotting analysis showed that in WT mice or heterozygous *S181A A/WT KI* mice, epinephrine treatment increased p53 expression in the heart, but no such effect was observed in homozygous *S181A A/A KI* mice (Supplementary Fig. 3e). Together, these data suggest that the *S181 A/A* mutation of RBM24 with a permanent impairment of the S181 phosphorylation has a gain-of-function effect that leads to enhanced RBM24-eIF4E complex formation, which inhibits the release of eIF4E from the complex, blocks p53 translation and reduces p53 expression level in *S181A A/A KI* mice.

To further characterize the molecular mechanism underlying the cardiovascular phenotypes in *S181A KI* mice, we performed a global genome-wide translation profiling assay, the Ribosome Nascent-chain Complex sequencing (RNC-seq), for H9C2 cells treated with Tat-Pep8 or scrambled Tat-Pep8-S. We identified 25 differentially translated mRNAs/genes (Fig. 3a), most of which contain a RBM24 binding mRNA motif (GUGUG or GAGUG) according to CISBP-RNA Database (http://cisbp-rna.ccbr.utoronto.ca/). Gene ontology (GO) analysis identified several major pathways, including muscle contraction and biology, lipoprotein metabolism and regulation, and cell cycle switching (Fig. 3a). RNA-ChIP analysis confirmed that RBM24 interacted with *Ankrd2*, *Apoe*, *Tmod4*, *Arhgef9*, and *Myh1* mRNAs (Fig. 3b). Western blotting analysis showed that Tat-Pep8 treatment increased the
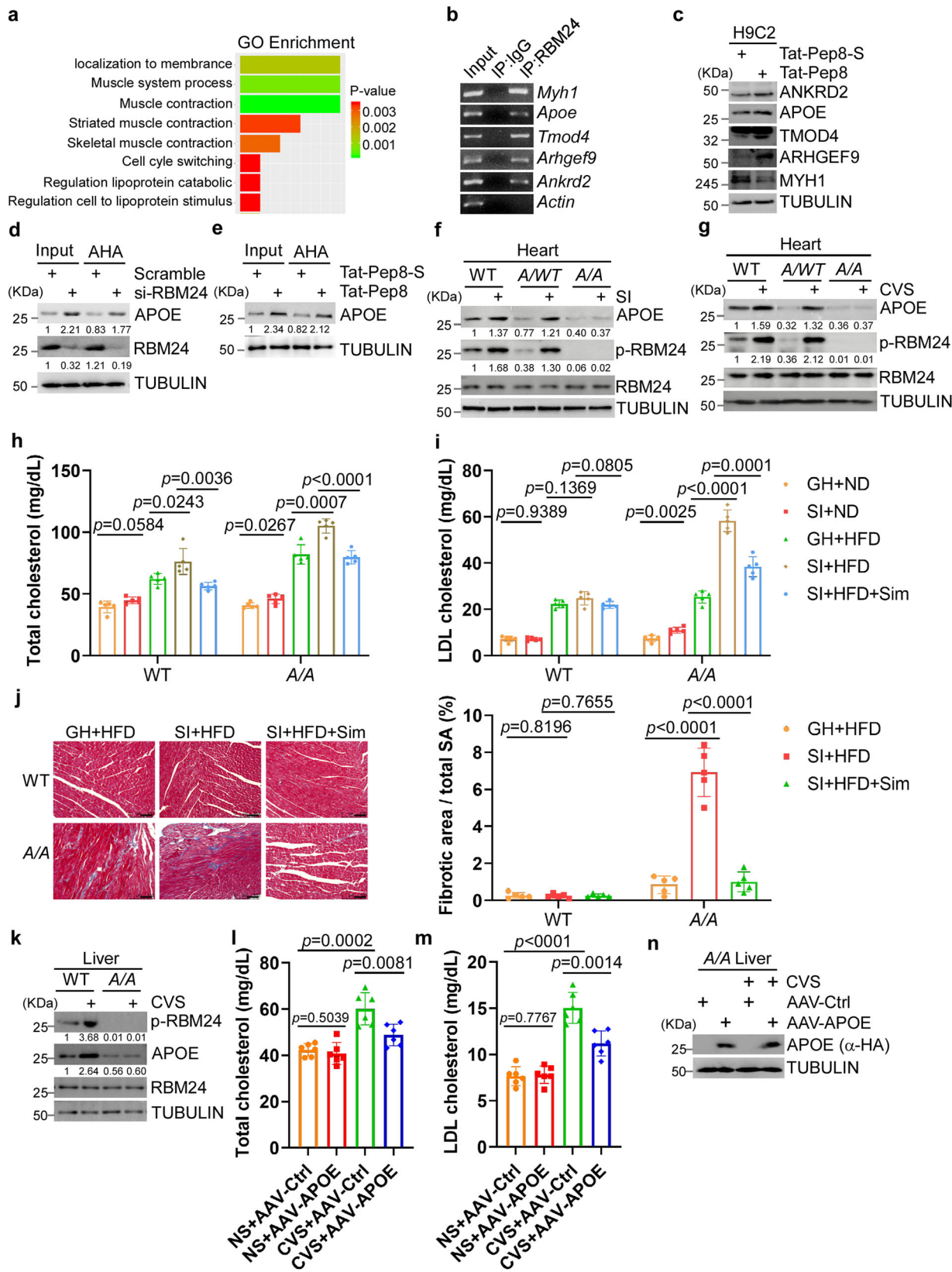
expression of proteins ANKRD2, APOE, TMOD4, and ARHGF9, but decreased the expression of MYH1 in H9C2 cells (Fig. 3c). The data suggest that in addition to p53 translation, RBM24 regulates the translation of many other proteins, including APOE.

Because genomic variants in *APOE* were associated with the risk of cardiovascular disease and dyslipidemia[46], we selected APOE for

follow-up analyses. An electrophoretic mobility shift assay (EMSA) for RNA-protein interactions showed that His-fused RBM24 formed a complex with the biotin-labeled *APOE* RNA probe (Biotin-ApoE-WT) that contains the GAGUG motif (Supplementary Fig. 3f). This RNA-protein complex formation was inhibited by an excess amount of unlabeled *APOE* probe (ApoE-WT cold probe), but not by unlabeled

**Fig. 3 | Impaired translation of APOE in *S181A KI* mice, leading to dyslipidemia.** **a** RNC-Seq was performed with H9C2 cells treated with Tat-Pep8 or Tat-Pep8-S. Differentially expressed genes ($p$ value <0.05, fold change >2, two-tailed unpaired Student's $t$-test) were analyzed for enriched biological processes via Gene Ontology. **b** RBM24-expressing H9C2 cells were subjected to immunoprecipitated with an anti-RBM24 antibody or IgG. The levels of indicated transcripts in immunocomplexes were determined by RT-PCR analysis ($n = 3$). **c** H9C2 cells were treated with Tat-Pep8 or scrambled Tat-Pep8-S for 24 h, followed by WB ($n = 3$). **d** Cells were treated with RBM24 siRNA or scrambled siRNA, then exposed to L-azidohomoalaine (AHA) and incubated with biotin/alkyne reaction buffer. Modified proteins were pulled down and analyzed by WB ($n = 3$). **e** Tat-Pep8 increased the translation of APOE. The experiment was as in (**d**) except that cells were treated with peptides for 24 h ($n = 3$). **f, g** SI and CVS increased APOE expression along with activation of S181

phosphorylation in mouse hearts. Mice were subjected to social isolation (SI) or group housing (GH) for 30 days (**f**), and CVS (chronic variable stress) or NS (nonstress) for 30 days (**g**) ($n = 3$). **h, i** SI increased the serum levels of total cholesterol (**h**) and LDL cholesterol (**i**) in *A/A* mice fed with HFD, ($n = 5$), Three-way ANOVA with Bonferroni post hoc correction for multiple comparisons. **j** Representative images of Masson's trichrome-stained heart sections (left) from (**h, i**) and corresponding quantification (right). Scale bars, 50 μm, ($n = 5$), Two-way ANOVA with Bonferroni post hoc correction for multiple comparisons. **k** CVS increased APOE expression along with activation of S181 phosphorylation in mouse liver, ($n = 3$). **l, m** APOE overexpression decreased the serum levels of total cholesterol (**l**) and LDL cholesterol (**m**) induced by CVS in *S181A KI* mice ($n = 6$), One-way ANOVA with Tukey's posttest. **n** Verification of HA-tagged APOE expression for (**l, m**) ($n = 3$). Data were shown as mean ± SD (**h–j, l, m**) from five to six independent experiments.

mutant *APOE* probe (ApoE-Mut cold probe) without the GAGUG motif (Supplementary Fig. 3f lanes 3 and 4). The specificity of this RNA-protein complex was confirmed further by supershift-EMSA with an anti-RBM24 antibody (Supplementary Fig. 3f lane5). The data indicate that RBM24 binds specifically to *APOE* mRNA, a prerequisite to its translation regulation.

An AHA-labeling translation assay showed that the level of newly synthesized APOE was increased by knockdown of *RBM24* (Fig. 3d) or Tat-Pep8 treatment of H9C2 cells (Fig. 3e). Then, we isolated rat cardiomyocytes and transfected plasmids expressing RBM24 WT, S181A, and S181D into the isolated cardiomyocytes. The results showed that both the WT and S181A mutant of RBM24 inhibited, while S181D activated, the expression of APOE (Supplementary Fig. 3g). Importantly, Western blotting analysis showed that the level of APOE in *S181A A/A KI* hearts was lower than that in WT or heterozygous *A/WT* hearts (Fig. 3f, g). Stress of SI or CVS increased the expression level of APOE in WT or heterozygous *A/WT* hearts, but not in *A/A* hearts (Fig. 3f, g).

Taken together, these data suggest that the *S181 A/A* mutation with a permanent impairment of the S181 phosphorylation of RBM24 reduces APOE amount in the cardiomyocyte of *S181A A/A KI* mice by inhibiting RBM24-mediated translation of APOE.

### Development of dyslipidemia in *S181A KI* mice

We suspected that *S181A KI* mice exhibited abnormal lipid metabolism. Indeed, 21-day SI stress significantly increased serum levels of total cholesterol (TC) and LDL cholesterol (LDL-C) in *S181A KI* mice, but not in WT mice, fed with a high-fat diet (HFD) (Fig. 3h, i). The effects were reversed by simvastatin, an inhibitor of HMG-CoA reductase, to lower cholesterols[47] (Fig. 3h, i). Interestingly, chronic variable stress (CVS) with heterotypic psychological stressors[48], significantly increased TC and LDL-C levels in *S181A KI A/A* mice, but not in WT mice, even when the mice were fed with a chow diet (ND) (Supplementary Fig. 3h, i). It is well-known that dyslipidemia is a key factor contributing to cardiac fibrosis and subsequent cardiovascular disorders. In line with this, combined SI stress and HFD feeding induced cardiac fibrosis in *A/A* mice, an effect blocked by simvastatin (Fig. 3j). In contrast, combined SI stress and HFD feeding did not induce cardiac fibrosis in WT mice (Fig. 3j). CVS alone for 40 days induced cardiac fibrosis in *A/A* mice, but not in WT mice, and the effect was blocked by simvastatin (Supplementary Fig. 3j).

We employed AAV9 (adeno-associated viruses) to facilitate the expression of APOE in *A/A* mouse cardiomyocytes via the cardiac troponin T (cTnT) promoter. However, we found that the overexpression of APOE in cardiomyocytes did not significantly regulate lipid metabolism. Given recent studies indicating RBM24's role in regulating liver lipid metabolism and that liver APOE mainly regulated lipid metabolism in the body, we examined whether RBM24 regulates APOE translation in the liver cell. L-azidohomoalaine (AHA) labeling assays showed that knockdown of RBM24 (Supplementary Fig. 3k) or Tat-Pep8 (Supplementary Fig. 3l) treatment increased the level of newly synthesized APOE (translation) in liver Hepa1–6 cells. More

importantly, we found that CVS stress-activated RBM24 S181 phosphorylation in the liver of WT mice, resulting in an increase in APOE expression, but not in *A/A* mice (Fig. 3k). AAV8-mediated APOE overexpression driven by the thyroxine-binding globulin (TBG) promoter in the liver partially contributed to the restoration of lipid metabolism in mice under CVS stress conditions (Fig. 3l–n). These findings suggest that stress induces dyslipidemia in *S181A KI A/A* mice, which may contribute to cardiac fibrosis and other cardiovascular disorders under chronic stress.

### APOE overexpression rescues *A/A* mice from acute stress-induced cardiac electrophysiological abnormalities

To investigate the mechanisms underlying acute stress-induced cardiomyocyte damage and cardiac electrophysiological abnormalities in *S181A KI* mice, we performed mass spectrometry experiments following three days of constitutive epinephrine injection (1 mg/kg, once daily) (Supplementary Fig. 4a). Under identical conditions, *A/A* mice exhibited a higher sensitivity to acute stress than WT mice, with 583 proteins differentially expressed in *A/A* mice and only 186 in WT mice (Supplementary Fig. 4b, c and Supplementary Data 1). Interestingly, pathway enrichment analysis revealed that the downregulated proteins in *A/A* hearts following stress were closely associated with mitochondrial function and lipid metabolism (Supplementary Fig. 4d and Supplementary Data 2). However, these two enrichment pathways with specific genes were absent in the altered proteins observed in WT mice. We also examined changes in protein expression of lipid metabolism-related genes, such as *PLIN2* and *ACSL3*[49], identified by MS in response to epinephrine injection. We found that epinephrine injection significantly inhibited the expression of these genes in *A/A* mice, whereas no comparable expression changes were observed in WT mice (Supplementary Fig. 4e).

Both mitochondrial function and lipid metabolism are associated with the function of APOE. Hence, we postulated that APOE had a significant role under acute stress conditions, as we examined the effect of epinephrine-induced acute stress on APOE expression. We found that epinephrine injection for 3 consecutive days (1 mg/kg, once daily) increased APOE expression in WT mice and *A/WT* mice, along with increased S181 phosphorylation, but not in *A/A* mice (Fig. 4a). Furthermore, we isolated primary cardiomyocytes from wild-type and *A/A KI* mice treated with epinephrine or saline as a control. The results showed that epinephrine increased the expression of APOE and p53, along with increased S181 phosphorylation of RBM24, in WT cardiomyocytes (Supplementary Fig. 4f). In contrast, these effects were not observed in *A/A KI* cardiomyocytes (Supplementary Fig. 4f). These findings suggest that APOE plays a significant role in cardiomyocytes during acute stress conditions.

Then, we overexpressed the APOE in *A/A* mouse cardiomyocytes driven by the cTnT promoter (Supplementary Fig. 4g). Our results showed that APOE overexpression prevented the upregulation of both Evans blue dye staining and Tn-1 expression that were induced by constitutive epinephrine injection (Fig. 4b, c). Most importantly, APOE
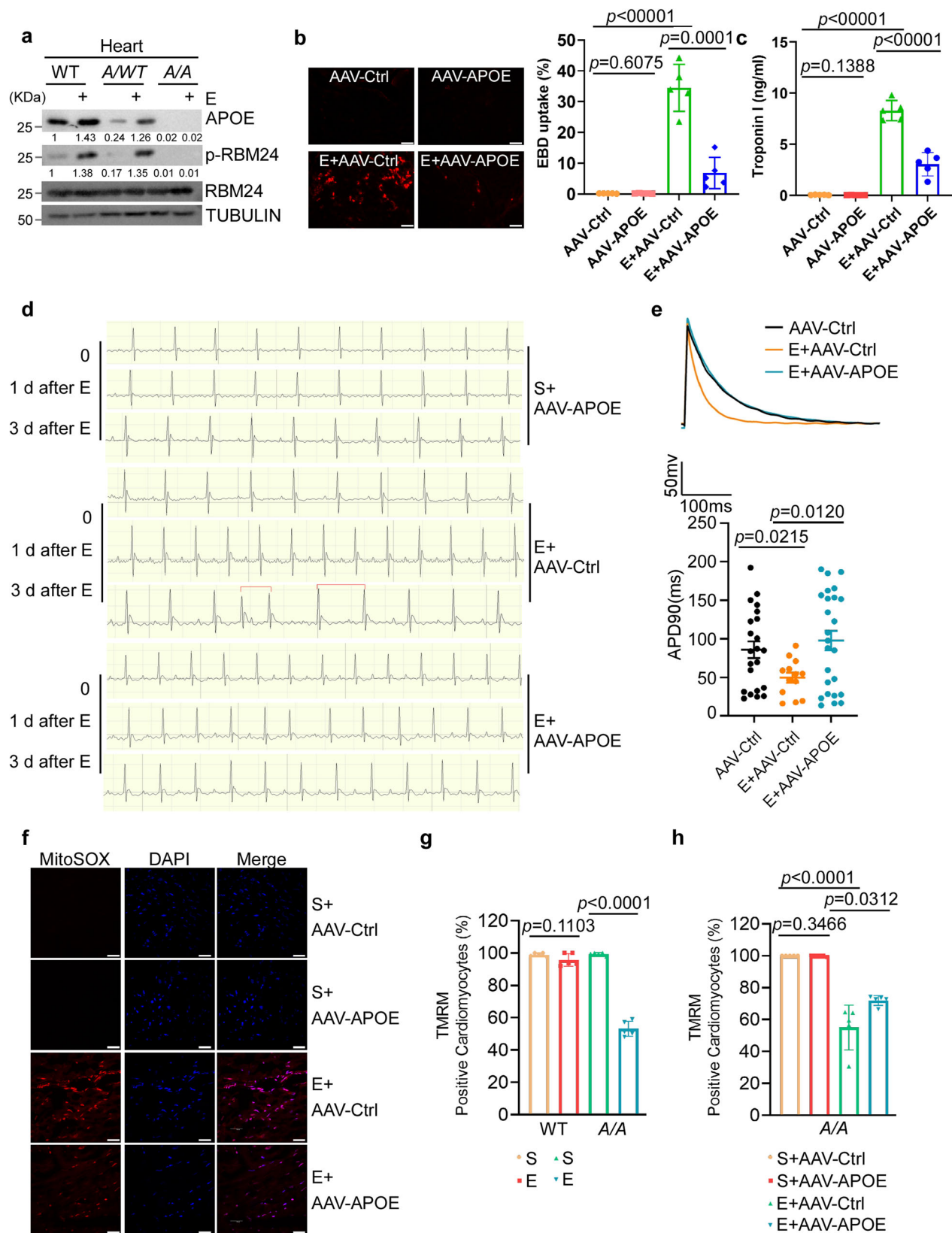
overexpression significantly inhibited electrophysiological abnormalities, including AF, following constitutive epinephrine injection (Fig. 4d and Table 2). We further quantified the action potential duration (APD) in mouse cardiomyocytes isolated from *A/A KI* mice, focusing on APD90—the time from the onset of a beat to 90% voltage repolarization[50]. Epinephrine treatment led to a significant reduction

in APD90 compared to the control (Fig. 4e). Notably, this effect is attenuated when APOE expression is upregulated (Fig. 4e and Supplementary Fig. 4e). This reduction in APD90, attributing to decreased APOE expression, tends to increase the occurrence of AF.

The mass spectrometry data suggest that mitochondrial dysfunction may occur in *A/A* mice under acute stress, which is a

**Fig. 4 | APOE overexpression rescues *A/A* mice from acute stress-induced cardiac electrophysiological abnormalities. a** Continuous injection of E induced APOE expression in WT and *A/WT* mice, but not in *A/A* mice (*n* = 3). **b** AAV9-mediated APOE overexpression rescues cardiomyocyte damage in *A/A* mice induced by continuous E injection. AAV9-cTnT-Ctrl (AAV-Ctrl) or AAV9-cTnT-HA-tagged-APOE (AAV-APOE, 3 × 10¹¹ viral genomes in 100 µl saline) was administered at 4 weeks of age. After 4 weeks, the mice received epinephrine (1 mg/kg/day) or saline for 3 days. Evans blue dye (EBD) uptake (left) and corresponding damage quantification (right) (*n* = 5). Scale bars, 50 µm. One-way ANOVA with Tukey's posttest. **c** AAV9-mediated APOE overexpression decreased Tn-I levels in *A/A* mice induced by continuous E injection. The treatment of mice as in (**b**), (*n* = 5), One-way ANOVA with Tukey's posttest. **d** AAV9-mediated APOE overexpression rescued *A/A* mice from acute stress-induced cardiac electrophysiological abnormalities. ECG was recorded before and 1 or 3 days after E injection (1 mg/kg/day), with/without

APOE overexpression (*n* = 4), The treatment of mice as in (**b**). **e** Action potential duration at 90% repolarization (APD90) was measured in cardiomyocytes derived from *A/A* mice. The treatment of mice as in (**b**). (AAV-Ctrl, *n* = 22 cells; E + AAV-Ctrl, n = 13 cells; E + AAV-APOE, *n* = 25 cells; 3 mice per group). One-way ANOVA with Tukey's posttest. **f** MitoSOX staining was performed on frozen heart sections in *A/A* mice to detect mitochondrial superoxide. The treatment of mice as in (**b**). Representative images were shown (*n* = 5). Scale bars, 30 µm. **g** TMRM staining of mitochondrial membrane potential in isolated cardiomyocytes from WT and *A/A* mice after 3 days of epinephrine (1 mg/kg/day) or saline (*n* = 5). Two-way ANOVA with Bonferroni post hoc correction. **h** TMRM staining of mitochondrial membrane potential in *A/A* mice cardiomyocytes after 3 days of epinephrine or saline injection (1 mg/kg/day), with/without APOE overexpression (*n* = 5). One-way ANOVA with Bonferroni post hoc correction. Data were shown as mean ± SD (**b**, **c**, **e**, **g**, **h**) from three to six independent experiments.

recognized precursor to reactive oxygen species (ROS) stress. ROS stress is a common stress signal associated with cardiac fibrosis and is directly linked to cardiomyocyte damage and cardiac electrophysiological abnormalities. To evaluate ROS levels in cardiac tissue, we used the mitochondrially targeted fluorescent dye, MitoSOX (2',7'-dichlorofluorescin diacetate), to measure superoxide production in mitochondria. We found that the hearts of *A/A* mice exhibited significantly elevated ROS levels compared to WT mice following continuous epinephrine injection (Supplementary Fig. 4i). Importantly, APOE overexpression attenuated ROS production in the heart of *A/A* mice, highlighting its protective role against oxidative stress (Fig. 4f).

Furthermore, we used tetramethyl rhodamine methyl ester (TMRM), a potential-sensitive fluorescent probe, to evaluate the mitochondrial membrane potential ($\Delta\Psi$m) in isolated cardiomyocytes, which is considered a reliable indicator of cellular mitochondrial function. We observed a significant decrease in mitochondrial membrane potential ($\Delta\Psi$m) in the hearts of *A/A* mice exposed to continuous epinephrine injection, compared to WT mice, suggesting mitochondrial membrane potential dissipation and mitochondrial dysfunction (Fig. 4g and Supplementary Fig. 4j). Importantly, overexpression of APOE prevented the decrease in mitochondrial membrane potential ($\Delta\Psi$m) in the hearts of *A/A* mice upon exposure to continuous epinephrine injection (Fig. 4h and Supplementary Fig. 4k).

Additionally, electron microscopic analysis revealed that cardiac mitochondria of *A/A* mice exposed to continuous epinephrine injection demonstrated disarray along the sarcomeres, with irregularities in cristae formation, whereas intact cristae were uniformly distributed across the organelle in the absence of epinephrine stress (Supplementary Fig. 4l). Notably, APOE overexpression ameliorated the mitochondrial structural abnormalities caused by acute epinephrine stress (Supplementary Fig. 4l). Our proteomic analysis revealed that acute epinephrine stress may suppress the expression of NDUFA1/NDUFA2 in *A/A* mice, but not in WT mice. These proteins play an essential role in mitochondrial function and the regulation of reactive oxygen species (ROS) production, and their deficiency can lead to mitochondrial dysfunction and ROS stress[51]. Importantly, we found that acute epinephrine stress inhibited the expression of NDUFA1/NDUFA2 in the hearts of *A/A* mice, and APOE overexpression restored them (Supplementary Fig. 4m). Conversely, acute epinephrine stress exhibited little effect on the expression of NDUFA1/NDUFA2 in the hearts of WT mice (Supplementary Fig. 4n). Collectively, these findings suggest that APOE plays a crucial role in preserving mitochondrial function in heart under acute stress, thereby preventing acute stress-induced cardiomyocyte damage and cardiac electrophysiological abnormalities.

### APOE overexpression rescues A/A mice from chronic stress-induced cardiac contractile dysfunction

We hypothesized that the inhibition of protein translation by *S181A mutation* was a key factor causing the severe cardiac abnormalities

observed in *A/A* mice. To test this hypothesis, we attempted to activate protein translation in the heart using Pep8, which impairs RBM24-eIF4E interaction as shown in supplementary Fig. 3a. A specialized TANNylated-Pep8 with a Tannic acid-modification[52] was intravenously delivered to *S181A KI* mice. Western blotting analysis showed that TANNylated-Pep8 increased expression of p53 and APOE in hearts of *S181A KI* mice compared with control TANNylated-Pep8-S (scrambled Pep8) (Supplementary Fig. 5a). Compared with *S181A KI* mice treated with saline and group housing (S + GH), those stressed mice by combined epinephrine and SI (E + SI) showed marked cardiac fibrosis, however, the effect was dramatically attenuated by TANNylated-Pep8 as compared to TANNylated-Pep8-S (Fig. 5a). Similar results were obtained with *S181A KI* mice under CVS (Supplementary Fig. 5b). Therefore, cardiac fibrosis in *S181A KI* mice under stress was reversed by TANNylated-Pep8 that inhibits RBM24-eIF4E interaction, but enhances translation and expression of APOE and other proteins.

Furthermore, we found that the overexpression of APOE via cTnT promoter suppressed cardiac fibrosis in *A/A* mice (Fig. 5b). Importantly, APOE overexpression prevented the decrease in left ventricular ejection fraction (LVEF%) and left ventricular fractional shortening (LVFS%) in *A/A* mice under E + SI stress conditions (Fig. 5c, d). Chronic stress may also lead to increased ROS stress in the hearts of *A/A* mice due to the inhibition of APOE. MitoSOX staining revealed elevated ROS levels in the hearts of *A/A* mice during the E + SI process, which was inhibited by APOE overexpression (Fig. 5e, f). These findings highlight the potential contribution of chronic stress-induced ROS stress to cardiac fibrosis and cardiac contractile dysfunction in *A/A* mice.

### Molecular mechanism for the S181 phosphorylation of RBM24

Previous studies have shown that GSK3β mediates RBM38 S195 phosphorylation[40]. Given that the RBM24 S181 site is homologous to RBM38 S195, it is possible that GSK3β also mediates phosphorylation at this site. To test this hypothesis, we treated H9C2 cardiac cells with GSK3β siRNA, leading to a reduction in GSK3β levels and subsequent inhibition of S181 phosphorylation (Supplementary Fig. 6a, b). Interestingly, treatment with either epinephrine or norepinephrine activated S181 phosphorylation of RBM24 in H9C2 cells (Supplementary Fig. 6c, d). However, GSK3β inhibitor lithium, prescribed for psychiatric disorders, inhibited epinephrine- and norepinephrine-induced RBM24 S181 phosphorylation[53] (Supplementary Fig. 6c, d). Similar results were obtained from the heart samples from mice with an intraperitoneal injection of epinephrine or norepinephrine compared with saline control (Fig. 6a, b), but not from other organs, including spleen, kidney, and lung (Supplementary Fig. 6e).

Similarly, acute stress with TMT increased the S181 phosphorylation of RBM24 in mouse hearts, and the effect was inhibited by lithium (Fig. 6c). Chronic stress by subjecting mice to SI for 30 days induced anxiety-like behaviors as indicated by decreased localization in the open field center as compared to the control mice with group housing (GH) (Fig. 6d). Serum epinephrine and norepinephrine levels in SI mice

**Table 2 | ECG characteristics from A/A mice treated with continuous epinephrine injection and overexpression APOE**

| Time (Days) | OE-APOE | | | E | | | E + OE-APOE | | |
|---|---|---|---|---|---|---|---|---|---|
| | 0 | 1 | 3 | 0 | 1 | 3 | 0 | 1 | 3 |
| HR (bpm) | 452±28 | 400±13 | 485±36 | 432±28 | 539±33 | 481±75 | 474±24 | 496±22 | 491±31 |
| PR (msec) | 40.4±3.9 | 46.3±4.8 | 43.8±3.5 | 42.3±2.1 | 44.4±3.2 | 48.5±11 | 46.2±2.7 | 48.6±4.41 | 49±5.2 |
| QT (msec) | 29.6±3.1 | 29.9±2.9 | 30.4±1.39 | 29.9±1.2 | 28.2±2.9 | 36.7±6.2 | 31.3±2.6 | 31.3±2.6 | 33.8±1.6 |
| QTc | 28.3±1.9 | 24.4±2.7 | 27.2±1.25 | 25.3±1.0 | 26.7±3.2 | 32.3±2.7 | 28.6±1.2 | 28.5±3.0 | 30.5±2.1 |
| QRS (msec) | 15.2±2.1 | 13.0±0.6 | 12.4±1.6 | 12.8±1.07 | 12.1±0.19 | 12.5±1.30 | 12.8±1.46 | 12.5±0.62 | 12.5±0.75 |
| AmpP (mv) | 0.11±0.01 | 0.08±0.01 | 0.08±0.01 | 0.09±0.01 | 0.07±0.01 | 0.06±0.01 | 0.08±0.02 | 0.09±0.01 | 0.09±0.03 |
| AmpQ (mv) | -0±0.01 | -0±0.01 | -0±0.01 | -0±0.01 | -0±0.01 | -0±0.01 | -0±0.01 | -0±0.01 | -0±0.01 |
| AmpR (mv) | 0.92±0.06 | 0.86±0.16 | 0.89±0.16 | 0.95±0.15 | 0.80±0.11 | 0.88±0.13 | 0.94±0.16 | 0.78±0.13 | 0.78±0.09 |
| AmpS (mv) | -0.18±0.05 | -0.08±0.01 | -007±0.01 | -0.06±0.08 | -0.06±0.02 | -0.06±0.02 | -0.06±0.02 | -0.04±0.01 | -0.05±0.01 |

HR heart rate, PR PR interval, QT QT interval, QTc QT interval corrected for HR, QRS QRS interval, AmpP amplitude of P wave, AmpQ amplitude of Q wave, AmpR amplitude of R wave, AmpS amplitude of S wave.

were significantly higher than that in GH mice (Supplementary Fig. 6f). The S181 phosphorylation of RBM24 was also increased in the hearts of mice after SI stress, and this effect was inhibited by lithium (Fig. 6e), but not in other tissues (Supplementary Fig. 6g). Consistently, AAV9-shGSK3 β-mediated GSK3 β knockdown obviously reduced RBM24 S181 phosphorylation in mouse hearts under SI stress conditions (Fig. 6f). Together, these results indicate that both acute stress and chronic stress-induced the S181 phosphorylation of RBM24 by GSK3β.

GSK3β was reported to bind and maintain proline-directed phosphorylation of RBM38 at S195, and its phosphorylation was activated by a hypoxic translation initiation factor eIF4E2[40]. As RBM24 is a paralog of RBM38, we hypothesized that stress-activated S181 phosphorylation of RBM24 was also through the eIF4E2-GSK3β-RBM24 signaling axis. Knockdown of eIF4E2 by two different siRNA downregulated the S181 phosphorylation of RBM24 in H9C2 cardiomyocytes (Fig. 6g and Supplementary Fig. 6h). Similarly, Tat-fused e2-I, a peptide that inhibits the eIF4E2-GSK3β interaction[40], inhibited the S181 phosphorylation of RBM24 in H9C2 cells in a concentration-dependent manner (Fig. 6h). Intravenous injection of TANNylated-e2-I inhibited the S181 phosphorylation of RBM24 in the mouse heart compared with TANNylated-e2-S (scrambled e2-I) (Fig. 6i). The data suggest that eIF4E2 and its interaction with GSK3β are important for the S181 phosphorylation of RBM24.

Then, we localized the RBM24-binding domain on eIF4E2 to the N-terminus (amino acid residues 1–15) as mutant GST-eIF4E2 with the deletion of amino acid residues 1–15 (Δ1–15) failed to pull down RBM24 in the GST pull-down assay (Fig. 6j). Peptide e2R-I corresponding to this domain was synthesized. Peptide e2R-I inhibited RBM24-eIF4E2 binding in GST pull-down assays (Fig. 6k). However, Tat-e2R-I peptide increased the S181 phosphorylation of RBM24 in H9C2 cells (Fig. 6l). Intravenous injection of TANNylated-e2R-I increased the S181 phosphorylation in hearts compared with TANNylated-e2R-S (scrambled e2R-I) (Fig. 6m). Our findings suggest that eIF4E2 plays a crucial role in regulating the S181 phosphorylation homeostasis of RBM24 through a delicate balance between the eIF4E2-GSK3β interaction, which activates S181 phosphorylation of RBM24, and the eIF4E2-RBM24 interaction, which inhibits S181 phosphorylation of RBM24.

### Constitutively active RBM24 phosphorylation induces cardiac abnormalities in mice with tamoxifen-inducible S181D mutant RBM24

To comprehensively characterize the physiological role of RBM24 S181 phosphorylation, we also studied the physiological role of S181D mutant RBM24 with constitutively active RBM24 phosphorylation. Since the disruption of RBM24 S181 phosphorylation is detrimental to cardiac structure and function in *S181A KI* mice (Fig. 1), we hypothesized that constitutively active RBM24 phosphorylation was beneficial to cardiovascular health. We created mice with tamoxifen (TAM)-inducible S181D RBM24 by using CRISPR/Cas9-mediated genome editing with homology-directed repair (HDR) (Fig. 7a, b). Surprisingly, opposite to our expectation, S181D mice showed cardiac dilatation and wall thinning (Fig. 7c, d).

We also treated mice with TANNylated-e2R-I, a peptide that constitutively activates the S181 phosphorylation of RBM24, and TANNylated-e2R-S as the negative control. Masson's trichrome staining of heart sections showed severe cardiac fibrosis one month after the treatment with TANNylated-e2R-I compared with TANNylated-e2R-S (Fig. 7e). Cardiac permeability assays with Evans blue staining showed dramatically increased permeability with TANNylated-e2R-I treatment compared with TANNylated-e2R-S treatment (Fig. 7f), indicating severe myocardial cell membrane damages. Myocardial cell damages with TANNylated-e2R-I treatment were also shown with increased serum Tn-I levels (Fig. 7g). Peptide e2R-I constitutively activated the S181 phosphorylation of RBM24, and led to the activation of p53 in H9C2 cells or in mouse hearts (Fig. 7h, i).
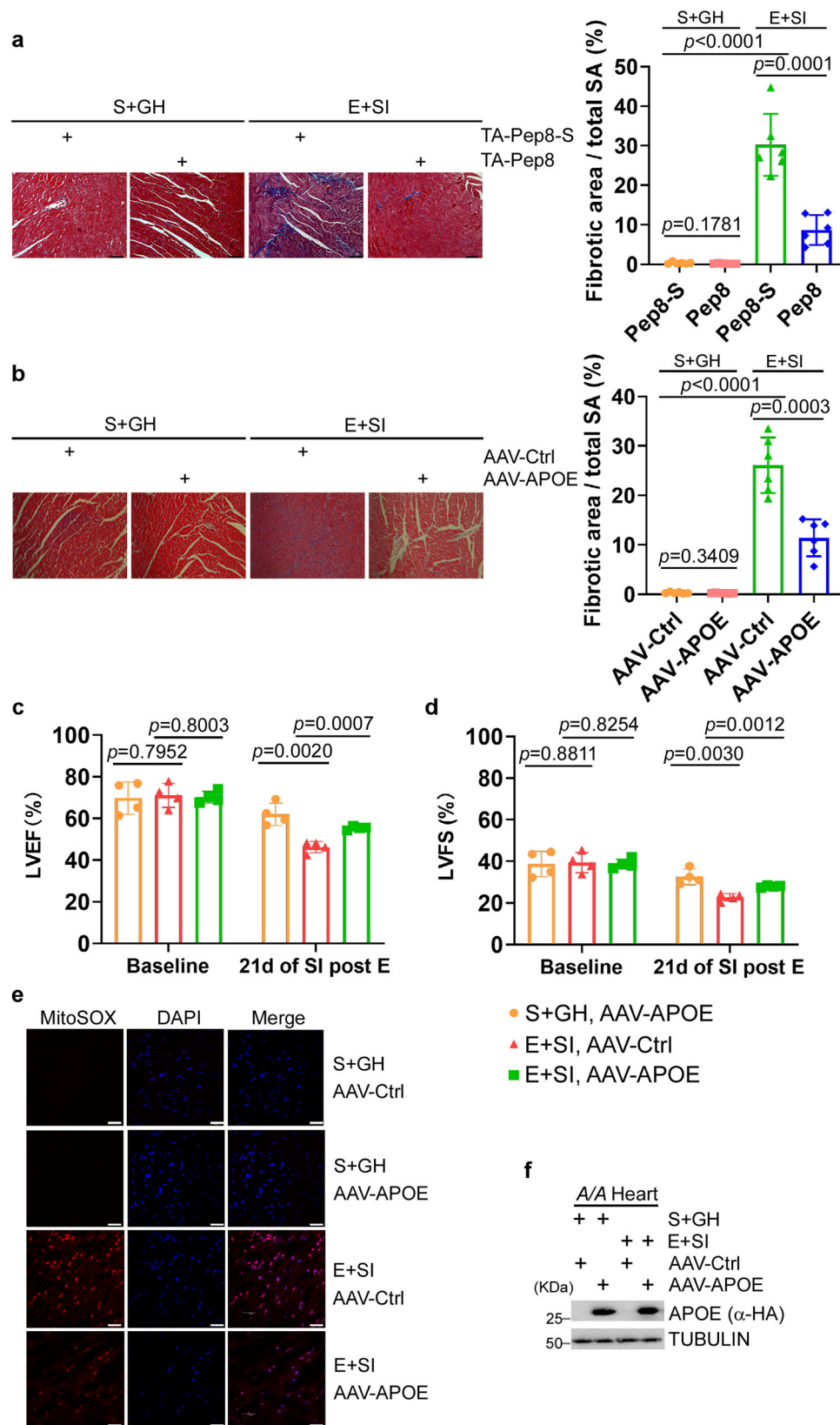
As sustained phosphorylation can ultimately be harmful to the heart, prolonged stress exposure in WT mice was expected to have detrimental effects on the heart. To investigate this, we subjected WT mice to a prolonged stress treatment, which included a combination of SI stress and random CVS stress to avoid adaptation. As a result, we observed mild cardiac fibrosis in WT mice after six months (Supplementary Fig. 7a). Interestingly, intermittent lithium treatment during the prolonged stress was found to alleviate cardiac fibrosis in WT mice (Supplementary Fig. 7a). Moreover, it was consistent that prolonged stress increased S181 phosphorylation of RBM24 in the heart of WT mice, which was alleviated by intermittent lithium treatment (Supplementary Fig. 7b). Collectively, these data demonstrate a

**Fig. 5 | APOE overexpression rescues *A/A* mice from chronic stress-induced cardiac fibrosis and contractile dysfunction. a** TANNylated-Pep8 (TA-Pep8) reduced stress-induced cardiac fibrosis in *A/A* mice. The mice were intraperitoneally injected with epinephrine (E) or saline (S), subjected to SI or GH, and then injected intravenously with TA-Pep8 or TA-Pep8-S. Representative images of Masson's trichrome-stained heart sections are shown at the left and quantification of the fibrosis area was shown at the right (*n* = 6). Scale bars, 50 μm, two-way ANOVA with Tukey's posttest. **b** AAV9-mediated APOE overexpression mitigated stress-induced cardiac fibrosis in *A/A* mice. Negative control AAV9-cTnT-Ctrl (AAV-Ctrl) or AAV9-cTnT-HA-tagged-APOE (AAV-APOE, 3 × 10^11 viral genomes in 100 μl saline) was administered by intrathoracic injection at 4 weeks of age. After 4 weeks, the mice were exposed to E + SI or S + GH, and heart tissue samples were collected three weeks later. Representative images of Masson's trichrome-stained heart sections are shown at the left and quantification of the fibrosis area was shown at the right (*n* = 6). Scale bars, 50 μm, two-way ANOVA with Tukey's posttest. **c**, **d** AAV9-mediated APOE overexpression rescued *A/A* mice from stress-induced contractile dysfunction. The left ventricular ejection fraction (LVEF) (**c**) and left ventricular fractional shortening (LVFS) (**d**) were analyzed at baseline and 21 days of SI post E, with or without APOE overexpression as indicated. The treatment of mice was as described in (**b**), (*n* = 4), two-way ANOVA with Bonferroni post hoc correction for multiple comparisons. **e** MitoSOX staining was performed on frozen heart sections in *A/A* mice. The treatment of mice was as described in (**b**). Representative images of the MitoSOX-stained heart sections were shown (*n* = 5). Scale bars, 30 μm. **f** WB analysis was conducted to verify HA-tagged APOE expression for (**e**) (*n* = 3). Data were shown as mean ± SD (**a**–**d**) from four to six independent experiments.

remarkable dose-effect relationship of RBM24 phosphorylation where it is essential for a protective effect on the heart in response to psychological stress, yet continuous activation can lead to cardiac harm.

### Serum S181 phosphor-RBM24 acts as a marker for mental stress in animals

Two types of antibodies were developed to specifically recognize S181 phosphor-RBM24 and non-phosphorylated RBM24, respectively. The phosphorylation antibodies were found to recognize S181D mutant RBM24 mimicking constitutively active S181 phosphorylation of RBM24, while not recognizing S181A mutant RBM24 (Supplementary Fig. 7c). The specificity of the phosphorylation antibodies was validated with Western blotting analysis in H9C2 cardiomyocytes with RBM24 knockdown, and the hearts from wild type and cardiac-specific conditional *RBM24* knockout (RBM24cKO) mice as well as calf intestine alkaline phosphatase treatment (Supplementary Fig. 7d–f). More importantly, we used the phosphothreonyl-tRNA synthetase-tRNA^CUA pair to synthesize S181-phosphorylated RBM24, mediated by the stop codon UAG at site 181[54]. We found that phosphorylation antibodies could detect S181-phosphorylated RBM24, while non-phosphorylation antibodies could not (Supplementary Fig. 7g).

Western blotting analysis with the phosphor-RBM24 antibody showed that S181-phosphorylated RBM24 was detectable in mouse serum samples after mental stress of SI in a time-dependent manner (Fig. 7j). Serum S181-phosphorylated RBM24 was easily detectable at day 10 and dramatically increased at day 30 (Fig. 7j). Co-immunoprecipitation was performed with the S181 phosphor-RBM24 antibody, and showed specific bands in serum samples of mice with TAM-inducible S181D expression (Supplementary Fig. 7h). The specific bands were confirmed to be RBM24 by Western blotting analysis or mass spectrometry. Similar results were obtained from rats or rabbits after SI stress (Supplementary Fig. 7i, j). Non-phosphorylation antibodies failed to detect RBM24 in the serum. We propose that phosphorylation promotes the release of RBM24 into the bloodstream while inhibiting recognition by non-phosphorylation antibodies. The data indicate that serum S181 phosphor-RBM24 is a biomarker for mental stress in mice, rats, and rabbits.

### Serum S181D RBM24 acts as a marker for mental stress in human

As a conscious species, humans are extraordinarily social, and being alone, even for a short period, has profound effects[55,56]. We ascertained ten healthy volunteers aged 20–30 and analyzed their serum RBM24 S181 phosphorylation levels before and after 10 h of social isolation. We enriched the phosphorylation proteins in serum samples via immobilized metal affinity chromatography (IMAC), and then measured the RBM24 S181 phosphorylation levels using Western blotting analysis. The serum S181 phosphorylation level of RBM24 was increased after SI stress for each participant, and the difference was statistically significant (Fig. 7k). Receiver operating characteristic (ROC) curve analysis was used to assess the discriminative ability of p-RBM24 in identifying psychological stress. The analysis

demonstrated a statistically significant association between p-RBM24 and psychological stress, with an area under the curve (AUC) of 0.94 (*p* < 0.001) (Fig. 7l). Furthermore, we found that the serum epinephrine and norepinephrine levels of the participants increased after 10 h of social isolation, indicating a positive association between psychological stress response and RBM24 phosphorylation activation (Supplementary Fig. 7k). In addition, RBM24 S181 phosphorylation was undetectable in serum samples after exercise. Similarly, in mice, RBM24 S181 phosphorylation was undetectable in serum samples after epinephrine injection or TMT induction, implying that the release of serum S181 phospho-RBM24 into the bloodstream might require a certain degree of accumulation. Nevertheless, given the specific association of RBM24 phosphorylation with the heart, it has the potential to serve as a biomarker for the effects of mental stress on human heart health.

## Discussion

Numerous population-based studies identified many psychosocial risk factors such as depression, anxiety, social isolation and lack of social support, acute stress (e.g., bereavement, earthquakes, war, and anger), and chronic stress (e.g., work-related stress, loss of job, and stressful life events) as potent risk factors for CVD[57]. However, the molecular mechanisms underlying these relationships remain unclear, posing challenges for the development of effective interventions.

### The phosphorylation of RBM24 links psychological stress to cardiovascular diseases

Multiple population-based studies suggested that psychological stress was associated with adverse outcomes in heart failure[58,59]. Acute emotional or psychological stressors may trigger Takotsubo syndrome or Takotsubo cardiomyopathy, characterized by an acute coronary syndrome, ST-elevation myocardial infarction (MI), and severe reversible left ventricular dysfunction without significant obstruction on coronary arteries[60]. A 4-year follow-up study of 6,808 individuals found a dose-response relationship between increasing optimism and decreasing heart failure incidence, and optimists had about half the risk of heart failure compared to pessimists[61]. Consistent with these findings in human patients, left ventricular dysfunction was observed in *Rbm24 S181A KI* mice 21 days after treatment of lose-dose epinephrine and social isolation (Fig. 1f, g).

Different from Takotsubo cardiomyopathy, that often shows a prolongation of QTc[62], ECG recordings showed QTc shortening in *Rbm24 S181A KI* mice after stress (Table 1). Interestingly, a genome-wide association study using 15,997 Hispanic/Latino individuals showed that genomic variant rs1320997, located 74,925 bp from *RBM24*, was positive association with the QT interval (*p* = 2.69 × 10^{-7}, β = 2.27)[63]. These findings suggest that RBM24 plays a role in determining the length of the QT interval on ECG, which is regulated by its phosphorylation status. Thus, impaired RBM24 phosphorylation may serve as the molecular basis for the impact of psychological stress on CVD.
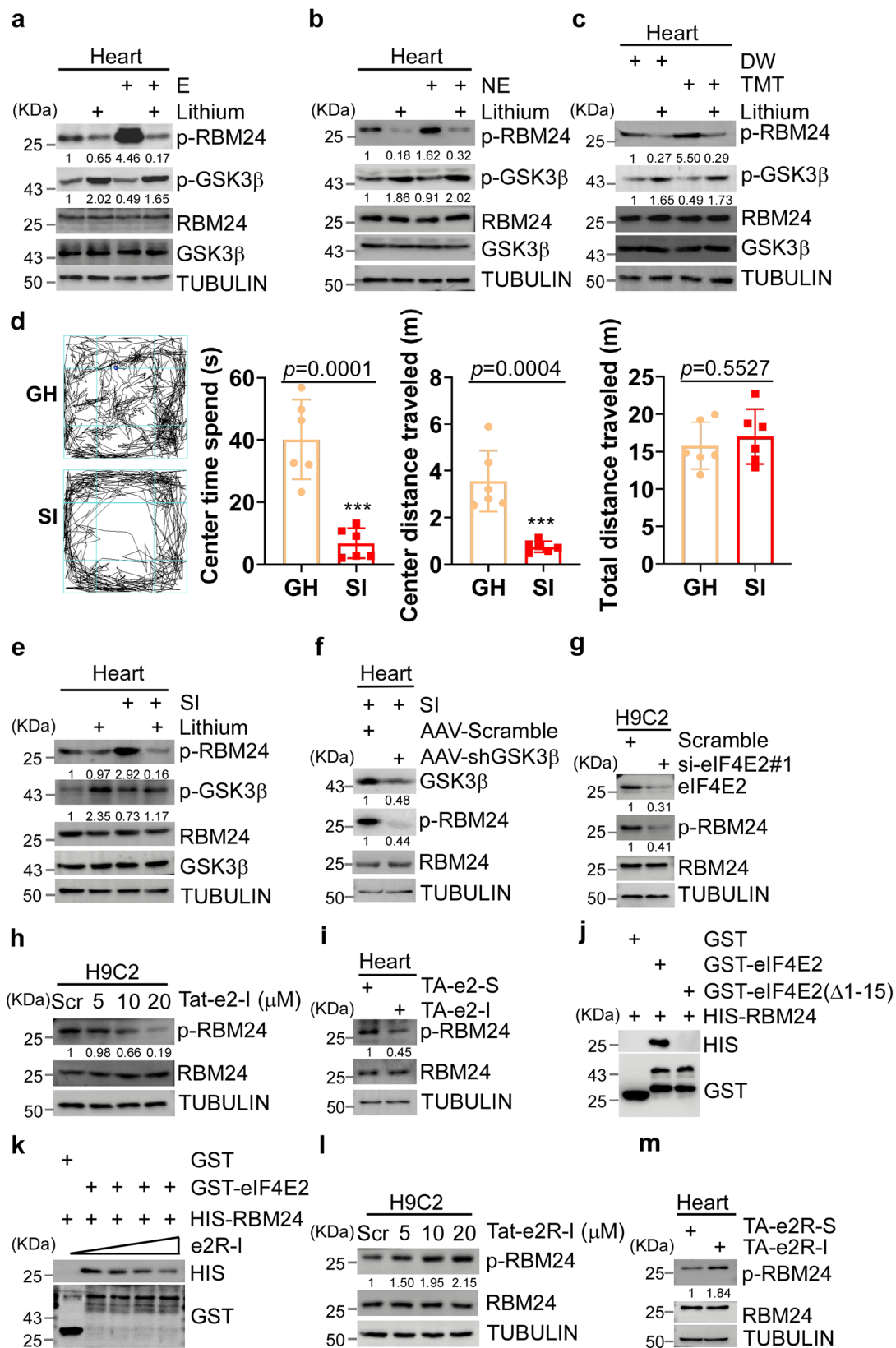
## Impaired RBM24 phosphorylation underlies psychological stress-induced arrhythmias

Mental stress is a well-known major trigger of cardiac arrhythmias and sudden death[64]. Studies have shown that psychological stress increases mortality and causes significant deterioration in both the structure and function of the heart in mice with arrhythmogenic cardiomyopathy (ACM)[65]. Anger and other negative emotions triggered potentially lethal ventricular arrhythmias (VT) and sudden cardiac death (SCD)[66]. Moreover, physical or emotional stress precipitated VT and SCD in patients with type 1 and type 2 long QT syndrome (LQT1, LQT2) and catecholaminergic polymorphic ventricular tachycardia (CPVT), whereas LQT3 patients and patients with

**Fig. 6 | Stress induces S181 phosphorylation of RBM24 in the heart. a, b** Mice were pretreated with lithium (4 mmol/kg) or saline for 6 h, followed by E (**a**) or NE (**b**) (5 mg/kg) injection. Heart tissues were collected for WB analysis ($n = 3$). **c** The experiments were done as in (**a**) except that after lithium pretreatment, mice were exposed to 5,5-dihydro-2.4. 5-trimethylthiazoline (TMT) or distilled water (DW) for 10 min ($n = 3$). **d** Mice under social isolation (SI) showed fewer entries and spent less time in the open field center compared to group housing (GH) mice. Locomotion tracks (left) and quantification of center time, center distance, and total distance traveled (right) were shown ($n = 6$), two-tailed unpaired Student's $t$-test, Data were shown as mean ± SD from six independent experiments. **e** Mice underwent SI or GH, and received intraperitoneally lithium (1 mmol/kg) or saline every 3 days for 30 days. Heart tissues were collected for WB analysis ($n = 3$). **f** Mice received AAV9-Scramble or AAV9-ShGSK3β ($1 \times 10^{12}$ viral genomes, 100 μl). After 4 weeks, followed SI or GH. Heart tissues were analyzed by WB ($n = 3$). **g** H9C2 cells were transfected with eIF4E2 or scrambled siRNA for 72 h, followed by WB ($n = 3$). **h.** H9C2 cells were treated with Tat-e2-I (5, 10, 20 μM) or scrambled e2-I (20 μM) for 24 h and analyzed by WB ($n = 3$). **i** Mice were injected with TANNylated-e2-I (TA-e2-I) or TA-e2-S (0.5 mM peptide, [TA]/[peptide] ratio of 5), and heart tissues were collected 6 h later for WB analysis ($n = 3$). **j** RBM24 interacted with eIF4E2 but not with the eIF4E2(Δ1–15) mutant. GST-eIF4E2, GST-eIF4E2(Δ1–15), or GST bound to GST-agarose beads were incubated with His-RBM24, and the elution was analyzed by WB ($n = 3$). **k** The purified GST-eIF4E2 was incubated with different concentrations of e2R-I, and incubated with purified His-RBM24, followed by WB ($n = 3$). **l** H9C2 cells were treated with different concentrations of Tat-e2R-I (5, 10, 20 μM) or scrambled e2R-I (Scr, 20 μM) for 24 h and analyzed by WB ($n = 3$). **m** Mice were intravenously injected with TANNylated-e2R-I (TA-e2R-I) or TA-e2R-S. 6 h later, heart tissues were collected and analyzed by WB ($n = 3$).

Brugada syndrome were more likely to develop VT and SCD during sleep or at rest[64]. Depression, anxiety, and hopelessness were linked to VT and SCD[57]. Consistent with the human data, our data showed that *S181A KI* mice died suddenly after social isolation and low-dose epinephrine treatment (Fig. 1e), indicating a causal role of psychological stress in sudden death using animal models.

AF is the most common arrhythmia seen in the clinical setting and increases the risk of stroke, heart failure, and sudden death. Although the link between psychological stress and VT and SCD is well-established, the data linking psychological stress to AF are mostly anecdotal or from small series[67]. Levy et al showed that in a small population of 756 AF patients, 51 patients had recurrent AF, with exercise or emotional stress was the precipitating factor for ten patients[68]. Lampert et al characterized 95 AF patients and found that stress, sadness, anxiety, anger, and impatience increased the risk of AF with odds ratios of >4, whereas happiness had a protective effect with an odd ratio of 0.12[69]. In a population of 378 patients with AF, Thompson et al showed that increased anxiety or depression was associated with increased symptom severity of AF[70]. Large-scale population studies also showed an association between AF and psychosocial stress, negative affectivities like depressed mood, vital exhaustion, and job strain[71]. We found that disruption of the S181 phosphorylation of RBM24 caused electrophysiological abnormalities, including reduced P wave amplitude, decreased QTc, and AF under acute stress (Fig. 1d). Our data demonstrate a causal role of psychological stress in AF, and define impaired RBM24 phosphorylation as a molecular basis for the impact of psychological stress on AF.

## APOE overexpression prevents psychological-stress-induced cardiovascular abnormalities by mitigating mitochondrial dysfunction and ROS Stress

The molecular mechanism underlying stress-induced heart failure, VT, AF and dyslipidemia is unknown, however, our data in this study provide important insights. We found that RBM24-S181 phosphorylation disruption caused profound impairment of the translation of many proteins involved in muscle contraction and biology and lipoprotein metabolism and regulation, including APOE, by affecting the binding of RBM24 to target mRNAs and translation initiation factor eIF4E (Fig. 3).

Our data suggest that reduced translation and expression of APOE in cardiomyocytes is the key to psychological stress-induced cardiac electrophysiological abnormalities, fibrosis, and contractile dysfunction in *S181A KI* mice. Previous studies have shown that *ApoE−/−* KO mice showed cardiac hypertrophy, left ventricular dilatation, and reduced ejection fraction than wild-type mice, which were associated with extensive interstitial and perivascular fibrosis[72]. *ApoE−/−* KO mice fed with a Western diet also showed significant age-dependent increases in TC, LV wall thickness, myocardial cell diameter, and LV collagen content (fibrosis)[73]. Cardiac fibrosis is a substrate for various myocardial diseases, including left ventricular dysfunction and heart failure[74]. Our

present study provides compelling evidence that reduced APOE expression in cardiomyocytes results in a surge of reactive oxygen species and mitochondrial dysfunction in response to both acute and chronic psychological stress (Figs. 4, 5). Acute epinephrine stress significantly reduces the action potential duration (APD) in cardiomyocytes derived from *A/A KI* mice, attributable to reduced APOE expression (Fig. 4e). Mitochondrial dysfunction and ROS stress likely explain this decrease in APD, potentially leading to AF onset in *A/A KI* mice[75]. The role of oxidative stress in the initiation and perpetuation of AF is well-established, and as such, antioxidant drugs have demonstrated favorable effects on AF development[76,77]. Moreover, impaired mitochondrial function compromises energy production, alters calcium handling, and instigates oxidative stress and inflammation, all of which contribute significantly to cardiac pathology, resulting in cardiac hypertrophy, heart failure (HF), cardiac ischemia–reperfusion injury, QT interval prolongation, T-wave abnormalities, sudden death, and AF[78,79]. Our results demonstrate that the overexpression of APOE can prevent the occurrence of cardiac electrophysiological abnormalities, fibrosis, and contractile dysfunction by mitigating mitochondrial dysfunction and ROS stress (Figs. 4, 5).

The relationship between cardiac mitochondrial function and APOE is primarily linked to lipid metabolism. Early stages of ApoE deficiency reduce basal mitochondrial respiration in the heart due to accelerated lipid substrate oxidation[80]. Low-carbohydrate, high-fat diets promote intrinsic mitochondrial function but have negative effects in APOE-deficient mice [81]. Recent research has found that ApoE plays a crucial role in LDL-L5-induced mitochondrial dysfunction in cardiomyocytes by colocalizing with mitochondrial VDAC, leading to mitochondrial swelling[82]. Our study reveals that APOE directly regulates mitochondrial function under stress conditions, potentially through the regulation of mitochondrial proteins like NDUFA1/NDUFA2 (Supplementary Fig. 4l–n). The specific regulatory mechanisms of APOE on these proteins require further investigation.

Another noteworthy finding is that chronic stress significantly increased total cholesterol and low-density lipoprotein cholesterol in *Rbm24 S181A KI* mice (Fig. 3h, i and Supplementary Fig. 3g, h). Recent studies have found that RBM24 plays a role in maintaining proper cellular lipid homeostasis and prevents liver steatosis[38]. Thus, the dyslipidemia observed in *Rbm24 S181A KI* mice under psychological stress may be related to the protein's function in the liver (Fig. 3l–n). In humans, controversial data exist regarding lipid levels in individuals with post-traumatic stress disorder (PTSD) as compared with healthy controls, and a recent meta-analysis found that PTSD patients had higher levels of TC, LDL, and TG, but lower HDL than healthy controls[83]. Controversial data were also reported for lipid levels in patients with major depressive disorder (MDD), and another meta-analysis found higher TG, but lower TC and LDL in MDD patients than healthy controls[84]. Diet-induced obesity and psychological stress can interact synergistically, leading to a deterioration of heart structure and function, resulting in a marked decline in both systolic and
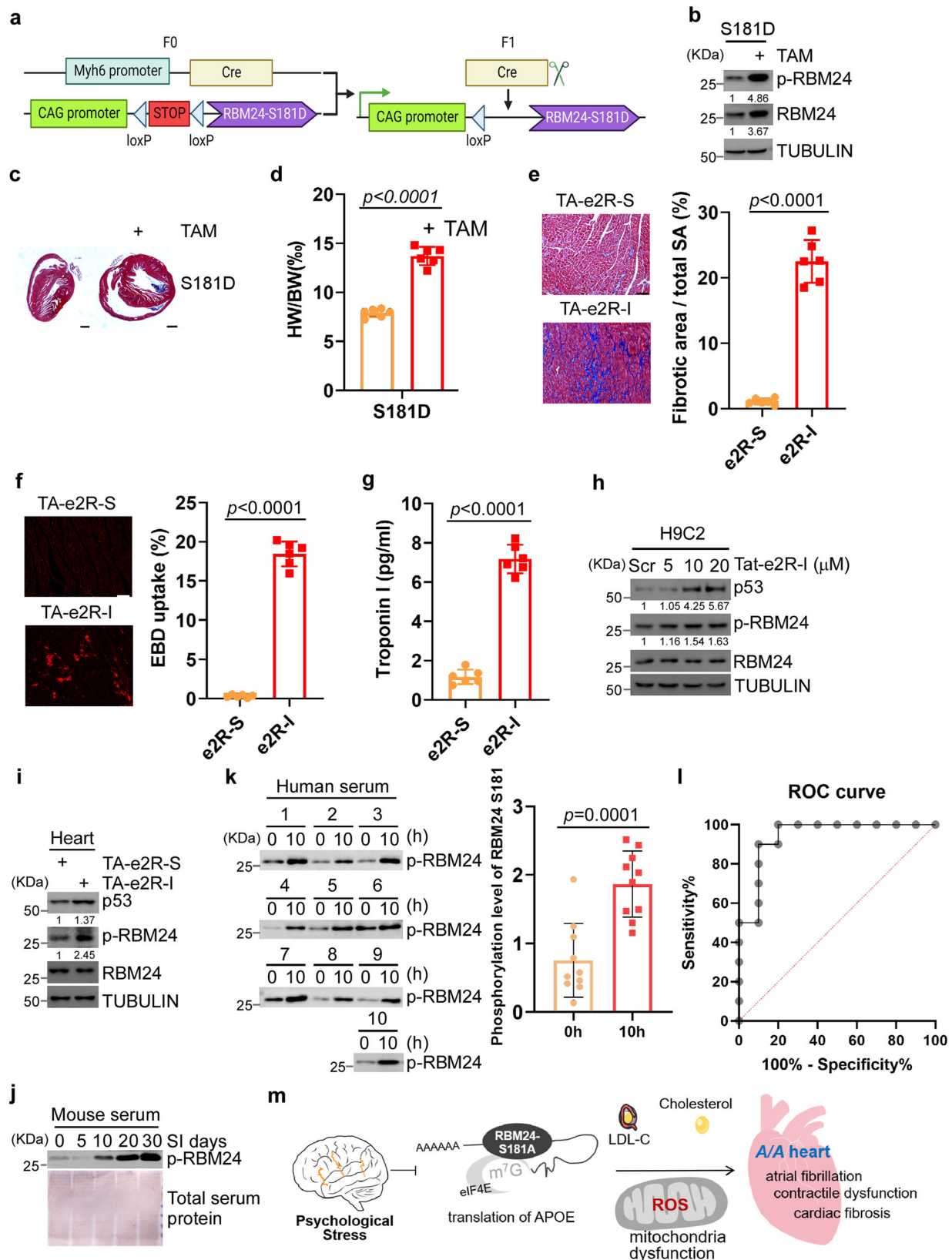
diastolic function[85]. Our study suggests that dyslipidemia caused by impaired RBM24-APOE axis, along with abnormal mitochondrial function or ROS stress, contributes to chronic stress-induced cardiac abnormalities.

Although the translation and expression of p53 was inhibited in *S181A KI* mice (Supplementary Fig. 3), this may not be critical to the cardiac phenotypes observed in these mice. Global *TP53* KO was shown to be protective of LV function, as doxorubicin treatment reduced LV fractional shortening and induced cardiac myocyte apoptosis in WT mice but not in *TP53* KO mice[86]. Endothelial-specific deletion of p53 improved cardiac function, reduced apoptosis of endothelial and non-endothelial cells, and decreased cardiac fibrosis[87]. However, the

**Fig. 7 | Constitutively active RBM24 phosphorylation induces cardiac abnormalities in mice with tamoxifen-inducible S181D RBM24. a** CRISPR/Cas9-mediated generation of *Rbm24* S181D conditional KI mice at the ROSA26 locus in C57BL/6 mice. **b** Conditional *Rbm24 S181D* KI mice were injected with tamoxifen (TAM) or corn oil for 5 consecutive days, and RBM24 expression in hearts was analyzed by WB ($n = 6$). **c** Masson's trichrome staining of heart sections from mice in (**b**). ($n = 6$), Scale bars, 1 mm. **d** Hearts weight/body weight (HW/BW) ratios of mice from (**c**) ($n = 6$). Two-tailed unpaired Student's *t*-test. **e** Mice received TA-e2R-I or TA-e2R-S every 4 days for 30 days. Masson's trichrome-stained heart sections (left) and fibrosis quantification (right) ($n = 6$). Scale bars, 50 μm. Two-tailed unpaired Student's *t*-test. **f** Evans blue dye (EBD) uptake images (left) and damage area quantification (right) are shown 6 days after TA-e2R-I or TA-e2R-S injection ($n = 6$). Scale bars, 50 μm. Two-tailed unpaired Student's *t*-test. **g** Troponin I (Tn-I) levels were measured in mice treated with TA-e2R-I or TA-e2R-S for 6 days ($n = 6$).

Two-tailed unpaired Student's *t*-test. **h** H9C2 cells were treated with different concentrations of Tat-e2R-I or scrambled e2R-S, and analyzed by WB ($n = 3$). **i** Mice were injected with TA-e2R-I or TA-e2R-S. After 6 h, heart tissue samples were analyzed by WB ($n = 3$). **j** Mice underwent social isolation for 5, 10, 20, and 30 days. Serum samples were collected and analyzed by WB. Congo red staining was used as a loading control ($n = 5$). **k** Serum samples were collected pre- or post-10h SI, enriched for phosphorylated proteins via IMAC (immobilized metal affinity chromatography), followed by WB analysis. Quantification of phosphorylation levels in serum was shown on the right ($n = 10$). Two-tailed unpaired Student's *t*-test. **l** The analysis of receiver operating characteristic (ROC) curves demonstrated a significant association between phosphorylated RBM24 (p-RBM24) and psychological stress (area under curve, AUC = 0.94, $p < 0.001$). The AUC value, *P* value were determined by ROC curve analysis. **m** Schematic illustration of the study's findings. Data were shown as mean ± SD (**d–f, g, k**) from six to ten independent experiments.

---

absence of p53, in combination with APOE deficiency, can synergistically promote the development of atherosclerosis[88]. Therefore, it is interesting to determine whether reduced p53 expression, in conjunction with APOE deficiency, may be linked to stress-induced dyslipidemia and other abnormalities, such as reduced muscle strength and abnormal behavior detected in *S181A KI* mice. In addition, increased p53 expression may be a key factor for cardiac fibrosis and dilatation observed in *S181D* mice and mice with constitute active S181 phosphorylation of RBM24 due to TANNylated-e2R-I injection (Fig. 7). We also showed that the inhibited interaction between RBM24 and eIF4E increased the translation and expression of ANKRD2, TMOD4, and ARHGF9, but decreased that of MYH1. Therefore, psychological stress may induce or aggravate cardiovascular diseases, muscle strength weakening, and abnormal behavior abnormalities in *S181A KI* mice by affecting the translation of these genes.

### RBM24 phosphorylation as a potential serum marker for chronic psychological stress

It is important to note that our studies with animal models (mice, rats, and rabbits) and human study subjects showed that the S181 phosphorylation level of RBM24 could serve as a biomarker for chronical psychological stress. The mental stress of social isolation induced dramatic increases in serum levels of S181-phosphorylated RBM24 in mice, rats, rabbits, and every human subject (Fig. 7j, k and Supplementary Fig. 7i, j). Therefore, a diagnostic test kit using active S181-phosphorylated RBM24 as a serum marker could enable easy and early detection of mental stress in individuals.

Interestingly, the S181 phosphorylation of RBM24 is a double-edged sword, as both its loss and constitutive active phosphorylation are detrimental to cardiac structure and function. Similar to *S181A KI* mice under stress, mutant S181D mice with constitutively active phosphorylation of RBM24 also showed cardiac dilatation and wall thinning (Fig. 7c, d), and TANNylated-e2R-I, a peptide that constitutively activates the S181 phosphorylation of RBM24, caused severe cardiac fibrosis, and dramatically increased permeability (i.e., severe myocardial cell membrane damages) (Fig. 7e–g). Thus, it is important to consider both constitutively active S181 phosphorylation of RBM24 and disruption of S181 phosphorylation in various physiological, pathological, and therapeutic contexts.

One of the major findings of this study is that RBM24-S181 phosphorylation can link psychological stress to cardiac diseases by regulating eIF4E-regulated translation. As a translation initiation factor, eIF4E is a prime target of translational control[89]. Both acute and chronic stress activated the S181 phosphorylation of RBM24 by GSK3β (Fig. 6a–c, e, f). This phosphorylation is tightly regulated by a complicated mechanism. First, eIF4E2 interacts with GSK3β through its C-terminal GSK3β-binding domain[40], mediating RBM24-S181 phosphorylation. Inhibiting this interaction by e2-I reduces this phosphorylation (Fig. 6g–i). Second, eIF4E2 also interacts with RBM24 through

its N-terminal domain, and inhibiting this interaction by e2R-I increases RBM24-S181 phosphorylation (Fig. 6j–m).

In summary, our study has discovered a critical signaling pathway that links psychological stress to cardiovascular disease by activating RBM24 S181 phosphorylation and regulating APOE translation. Dysregulation of this pathway leads to ROS stress, mitochondrial dysfunction, and dyslipidemia, contributing to cardiovascular disease under both acute and chronic stress conditions (Fig. 7m).

## Methods

### Reagents and plasmids

The used antibodies, other supplies, the cloning strategy, and primers used were listed in supplemental experimental procedures.

### Cell culture, transfection, and RNA interference

H9C2 were obtained from China Center for Type Culture Collection (CCTCC), and cultured in DMEM (Gibco) supplemented with 10% fetal bovine serum (FBS) (Hyclone), 100 units/ml penicillin, and 100 μg/ml streptomycin. H9C2 cells were cultivated at 37 °C in 5% $CO_2$ humidity. Plasmids or small interfering RNAs (siRNA) were transfected into cells according to the instructions from Thermo Fisher (L3000015, Lipofectamine 3000 Reagent). The small interfering RNAs (siRNA) include those targeting RBM24#1 (5′ CACUGGAGCCGCCUACGCA dTdT 3′), RBM24#2 (5′ AGAUAAAUAGAAAGACAA dTdT 3′), eIF4E2 #1 (5′ CUCACACCGACAGCAUCAA dTdT 3′), eIF4E2 #2 (5′ AUGAUCAGAAUGAAGAAACAGC dTdT 3′), and the scrambled control siRNA (5′ UUCUCCGAACGUGUCACGU dTdT 3′). GSK3β siRNA #1 (5′ GCAUUUAUCGUUAACCUAA dTdT 3′), GSK3β siRNA #2 (5′ACACGAAAGUGAUUGGAAA dTdT 3′), and the scrambled control siRNA (5′UUCUCCGAACGUGUCACGU dTdT 3′). GSK3β shRNA: (5′ GGCGACCGAGAACCACCUCCUUUGCGGAG 3′) along with a scramble control shRNA: (5′ UGACCACCCUGACCUA CGGCGUGC AGU GC 3′).

### Animal studies

RBM24 S181A knockin mice were generated on the C57BL/6N background by using gene targeting (Cyagen Biosciences, Guangzhou, China). The Animal Experimental Ethics Committee of Huazhong Agricultural University specifically approved the entire study with the approval number #HZAUMO-2018-006. The mice were housed in the animal facility at Huazhong Agricultural University. Mice were housed 4 per cage with ad libitum access to water and a standard chow diet (4% fat diet), or a high-fat diet (60.0% fat diet), and the housing environment was maintained at 22–24 °C with a 12 h light/dark schedule (lights on at 06:00 and off at 18:00). And humidity maintained between 40 and 60%. All animals received free access to food and water. For social isolation (SI) stress, 8-week-old C57BL/6 N mice were individually housed (socially isolated) in standard mouse cages. For short-term SI stress, mice of the same gender were used in the same experiment. For the 1-year social isolation experiment, both males and females were subjected to evaluation. In all

animal experiments, gender was consistent among the same group, and female and male groups were set up.

Transgenic mice with overexpression of RBM24 S181D were generated on the C57BL/6 background by using CRISPR-Cas9 technology (Cyagen Bioscience, Guangzhou, China). Briefly, C57BL/6 female mice were used as embryo donors and foster mothers. Superovulated 8-week-old female C57BL/6 mice were mated to C57BL/6 males, and the fertilized eggs from oviducts were collected. Cas9 and gRNA were co-injected into fertilized eggs with a targeting vector (CAG-loxP-Stop-loxP-kozak-mutant mouse Rbm24 CDS-polyA). Cardiac-specific overexpression of RBM24 S181D in mice were achieved by crossing RBM24 S181D overexpression mice to Myh6-Cre mice from Cyagen Biosciences.

### Chronic variable stress (CVS)

Mice were exposed to a protocol of various environmental stressors in a random order. Stressors included illumination during the TMT exposure (10 min), social defeat, cage tilt (45°, 4–6 h), overnight soiled cage bedding (14 h), white noise (80 db, 2–6 h), and/or shaking (150 rpm, 1 h). For social defeat, mice were introduced in a cage with an aggressive mouse, and after being defeated, they were placed in a transparent and perforated plastic container to avoid further physical contact and potential injury, and the plastic container retained in the resident home cage for 30 min. After 4 weeks of exposure to the stress protocol, mice were used for the next experiments.

### RNC sample preparation, mRNA-seq, and RNC-seq

H9C2 cells were treated with 10 μM Tat-Pep8 or Tat-Pep8-S (scramble peptide) for 24 h. Each sample group had three biological replicates. Each cell sample (-3 million) was treated with pre-chilled cell lysis buffer. The lysates were centrifuged at 12,000×$g$ for 20 min at 4 °C, and then the supernatants were transferred to 12.5 ml of sucrose buffer (30% sucrose in ribosome buffer (RB buffer) [20 mM HEPES-KOH (pH 7.4), 15 mM $MgCl_2$, 200 mM KCl, 100 mg/ml cycloheximide, and 2 mM dithiothreitol]. After centrifugation at 185,000×$g$ for 5 h at 4 °C, the pellet was suspended in cold RB buffer to obtain RNC. Each RNC sample was treated with Trizol to obtain RNC-mRNA. Total RNA was extracted using the Trizol Regent (Invitrogen, USA). Sequencing libraries were generated using VAHTS Universal V6 RNA-seq Library Prep Kit for Illumina (Vazyme, China) following the manufacturer's instructions and sequenced on an Illumina NovaSeq 6000 sequencer. High-quality reads that passed the Illumina quality filters were kept for the sequence analysis.

### Quantitative proteomics

WT and *A/A* mice were treated with 1 mg/kg epinephrine or PBS and continued for 3 days. Then, the hearts of the WT and *A/A* mice were collected and frozen in liquid nitrogen after continuous epinephrine injections. Three groups were treated with PBS in WT mice,

Three groups were treated with E in WT mice, three groups were treated with PBS in *A/A* mice, three groups were treated with E in *A/A* mice. Total 12 samples. The frozen tissue was ground into powder and sonicated three times in a lysis buffer containing 8 M urea, 1 mM PMSF, and 2 mM EDTA. The debris was removed by centrifugation at 15,000×$g$, and the protein concentration was determined using a BCA kit. Equal amounts of protein samples were digested with trypsin, and the supernatants were mixed with 8 M urea, reduced with 10 mM DTT, and alkylated with 50 mM Miodoacetamide. The protein samples were precipitated with chilled acetone, air-dried, and digested overnight at 37 °C in 25 mM ammonium bicarbonate solution with trypsin.

After digestion, peptides were desalted using a C18 Cartridge, followed by drying with a vacuum concentration meter, concentrated by vacuum centrifugation, and redissolved in 0.1% (V/V) formic acid. Then, liquid chromatography (LC) was performed on a nanoElute UHPLC (Bruker Daltonics, Germany). About 200 ng peptides were separated within 40 min at a flow rate of 0.3 uL/min on a commercially available reverse-phase C18 column with an integrated CaptiveSpray Emitter (25 cm × 75 μmID, 1.6 μm, Aurora Series with CSI, IonOpticks, Australia). The separation temperature was kept by an integrated Toaster column oven at 50 °C. Mobile phases A and B were produced with 0.1 vol.% formic acid in water and 0.1% formic acid in ACN. Mobile phase B was increased from 2 to 22% over the first 25 min, increased to 35% over the next 5 min, further increased to 80% over the next 5 min, and then held at 80% for 5 min. The LC was coupled online to a hybrid timsTOF Pro2 (Bruker Daltonics, Germany) via a CaptiveSpray nano-electrospray ion source (CSI). To establish the applicable acquisition windws for diaPASEF mode, the timsTOF Pro2 was operated in data-dependent parallel accumulation-serial fragmentation (PASEF) mode with 4 PASEF MS/MS frames in 1 complete frame. The capillary voltage was set to 1500 V, and the MS and MS/MS spectra were acquired from 100 to 1700 m/z. As for the ion mobility range (1/ $K0$), 0.85 to 1.3 Vs/$cm^2$ was used. The "target value" of 10,000 was applied to a repeated schedule, and the intensity threshold was set at 1500. The collision energy was ramped linearly as a function of mobility from 45 eV at 1/$K0$ = 1.3 Vs/$cm^2$ to 27 eV at 1/$K0$ = 0.85 Vs/$cm^2$. The quadrupole isolation width was set to 2 Th for m/z < 700 and 3 Th for m/z > 800. In diaPASEF mode, the instrument control software was extended to define quadrupole isolation windows as a function of the TIMS scan time. Seamless and synchronous ramping of all applied voltage is achieved by modifying the instrument control electronics. We defined 25 Th isolation windows from m/z about 400 to 1200, and totally 48 windows were defined. Other parameters were the same as DDA-PASEF mode.

MS raw data were analyzed using DIA-NN(v1.8.1) with library-free method. The uniprot-proteome_UP000000589_Mus_musculus.fasta database (A total of 55319 sequences) was used to create a spectra library with deep learning algorithms of neural networks. the option of MBR was employed to create a spectral library from DIA data and then reanalyse using this library. FDR of search results was adjusted to <1% at both protein and precursor ion levels, the remaining identifications were used for further quantification analysis. For the pathway enrichment analysis, we used MetaScape (https://metascape.org/gp/index.html).

### Preparation of TANNylated peptides for mouse studies

Preparation of TANNylated peptide[52], the tannic acid (TA) solution (10 mM), and peptide solution (0.5 mM) were prepared. The TA solution was diluted to 0.05, 0.1, 0.5, or 1 mM. The diluted TA solution and peptide solution were mixed vigorously at a volumetric ratio of 1:1, corresponding to the following stoichiometric ratios of [peptide]/[TA]: 10, 5, 1, and 0.5. The ratio of [peptide]/[TA] equal to 5 was the most appropriate. After 30 min of incubation at room temperature, 200 μl TANNylated-peptide solution was intravenously injected into mouse tail veins (8-week-old C57BL/6 N mice). For the short-term treatment, the mice were sacrificed 6 h after injection. For the long-term treatment, the mice were injected every four days for a month.

### Human social isolation

We performed short-term human social isolation[90], and the Human Experimental Ethics Committee of Huazhong Agricultural University approved the human subject research with the approval number #HZAUHU-2021-0004. Eligible participants were recruited through community flyers and word of mouth, and were screened to ensure they met the inclusion criteria. Upon arrival at the study site, participants provided written informed consent and completed a baseline questionnaire, including demographic information and medical history. Ten healthy adults (four females and six males) with a mean age of 26 years (age range: 20 to 30) were selected for the study. All participants had a BMI mean (standard deviation) of 21.9 (1.9), were within a healthy weight range (18–24), reported normal social interactions, and had no history of cardiovascular disease or medication use in the past 3 months. Participants were socially isolated for 10 h. On the day of

isolation, participants arrived at 8:00 a.m., and explained the precautions and requirements in detail. The use of mobile phones and computers were not allowed, but non-social games such as puzzles, sudoku coloring pages, drawing, and writing supplies were provided during the isolation. Approximately 5 ml of blood samples were collected. Then, the participants were isolated from 9:00 to 19:00 in a room with a chair, a table, enough water, and food. We set up a panic button in their rooms in case of an emergency. After 10 h, 5 ml of blood samples were withdrawn. Serum was isolated from the blood samples, enriched and concentrated by IMAC, and used for Western blot analysis.

### Purification of phosphoproteins by IMAC

Purification of phosphoproteins by IMAC was as described[91,92]. Briefly, POROS MC Metal Chelate Affinity Resin (Thermo Fisher Scientific, USA) in a 1.5 mL microtube was charged with 100 μL 100 mM $GaCl_3$ solutions. The resin was washed three times with 500 μL 0.1% acetic acid to remove unbound metal ions. Then, 200 μL serum samples were diluted with 1 mL 50 mM Mes/NaOH buffer (containing 0.5 M NaCl, pH 5.5), mixed, and incubated at 4 °C for 2 h. The resin was washed with 500 μL of the same buffer to remove nonspecifically bound proteins. Finally, phosphoproteins were eluted with 100 μL 0.2 M sodium phosphate buffer (pH 8.0) at 60 °C for 15 min. A total of 5 ml of serum samples were used for phosphoprotein enrichment, followed by trichloroacetic acid precipitation.

### Expression of phosphorylated RBM24 through genetic code expansion

The genetic code expansion technology was utilized in this study to express phosphorylated RBM24 in *Escherichia coli*[93]. The S181 residue of RBM24 was mutated to an amber codon and cloned into the pRSF protein expression vector. The engineered SepRS/tRNA pair (orthogonal aminoacyl-tRNA synthetase, Plasmid #173897) and pRSF-RBM24 mutant with the amber codon at position 181 were co-transformed into Escherichia coli BL21 ΔSerB strain. Phosphoserine analog (DL-AP4) was then utilized as a substrate to express phosphorylated RBM24 through arabinose induction at 16 °C, for 9 h.

### Isolation of primary mouse atrial cardiomyocytes and recording of atrial action potential duration

Mouse atrial cardiomyocytes were isolated using the Langendorff perfusion method as described by us previously[94]. In brief, a 6–8 weeks old mouse was pre-injected with 0.2 ml of heparin (1000 IU/ml) to prevent clotting, anesthetized, and sacrificed.[95] The heart was dissected out, washed with cold PBS, and hung on the Langendorff perfusion system. The perfusion was carried out with the Tyrode's solution containing (mM): 135 NaCl, 5.4 KCl, 0.33 $NaH_2PO_4.2H_2O$, 1.0 $MgCl_2$, 10 glucose, and 5 HEPES with pH adjusted to 7.2 with NaOH at 22 °C. The heart was then perfused with a "low $Ca^{2+}$, $Mg^{2+}$ free" solution containing *Clostridium histolyticum* collagenase (type II, Worthington Biochemical Corporation), elastase (Worthington Biochemical Corporation) and protease (type XIV, Sigma) for 25 min at 37 °C. The atrial tissue was cut and placed in 0.1% BSA, followed by incubation in 0.1% BSA with serial and incremental increases in $Ca^{2+}$ for a final concentration of 1 mM. Atrial myocytes were collected in 1.5 ml Eppendorf tubes by gravity sedimentation, and resuspended in recording bath solution for recording of action potentials[95].

The recording of the atrial action potential was performed using a MultiClamp 700 A amplifier connected to the digital-analog system Digidata 1440 A and pClamp 10.4 software (Axon Instruments) as described by us previously[95]. We selected only a single, rod-shaped, well-conditioned cell for recording. The borosilicate glass microelectrode with a length of 100 mm, an outer diameter of 1.5 mm, and an inner diameter of 0.84 mm was purchased from Chengdu Microprobe Scientific Instrument. When the electrode was injected into the liquid, the resistance was 2.0–3.0 MΩ. The internal pipette solution contained 150 mM NaCl, 4 mM KCl, 2 mM $CaCl_2.2H_2O$, 1.0 mM $MgCl_2$, 10 mM glucose, and 5 mM HEPES with pH adjusted to 7.2 with NaOH. The external solution buffer contained 140 mM KCl, 10 mM NaCl, 5 mM EGTA, 1.0 mM $MgCl_2$, and 10 HEPES with pH adjusted to 7.2 with KOH. Atrial cardiomyocytes were depolarized with a current step of 300–1300 pA and 3 ms duration at a cycle length (CLs) of 0.2 s. During recordings, zero holding current was applied, and each recording train consisted of 11 sweeps at the specified CL. Signals were low-passed filtered at 2 kHz, digitized at 10 kHz, and analyzed as described[94].

### Statistical analysis

All quantitative data were shown as mean ± s.d. The difference between two groups of variables was compared by the two-tailed, paired or unpaired Student's $t$-test. Comparisons of three or more groups were analyzed using one-way (one variable) or two-way (two variables) ANOVA followed by the Bonferroni post hoc correction for multiple comparisons when appropriate. A $P$ value of <0.05 was considered as significant. Quantification of cardiac fibrosis or EBD uptake was carried out by ImageJ.

The discriminative ability of phosphorylated RBM24 in identifying psychological stress was evaluated using ROC analysis. To accomplish this, the levels of RBM24 phosphorylation expression were quantified using ImageJ software from the Western blot of the same subject, before and after 10 h of social isolation, and the ROC curve was plotted accordingly. The receiver operating characteristic (ROC) curve was plotted by the GraphPad prism 8.0. The area under curve (AUC) was calculated by GraphPad 8.0. All statistical analyses were performed using GraphPad Prism 8.0 for Windows.

### Reporting summary

Further information on research design is available in the Nature Portfolio Reporting Summary linked to this article.

## Data availability

The RNA-Seq and RNC-Seq data in this study have been deposited in the Sequence Read Archive (SRA) under the project accession PRJNA703336. The heart mass spectrometry data obtained following epinephrine injection in this study have been deposited in the iProX using the dataset identifier PXD049058. The data supporting the findings from this study are available within the manuscript and its supplementary information. Source data are provided with this paper.

## References

1. Critchley, H. D. et al. Mental stress and sudden cardiac death: asymmetric midbrain activity as a linking mechanism. *Brain* **128**, 75–85 (2005).
2. Vancheri, F., Longo, G., Vancheri, E. & Henein, M. Y. Mental stress and cardiovascular health-part I. *J. Clin. Med.* **11**, 3353 (2022).
3. Song, H. et al. Stress related disorders and risk of cardiovascular disease: population based, sibling controlled cohort study. *BMJ* **365**, l1255 (2019).
4. Ziegelstein, R. C. Acute emotional stress and cardiac arrhythmias. *JAMA* **298**, 324–329 (2007).
5. Lambiase, P. D., Garfinkel, S. N. & Taggart, P. Psychological stress, the central nervous system and arrhythmias. *QJM* https://doi.org/10.1093/qjmed/hcad144 (2023).
6. Edmondson, D., Newman, J. D., Whang, W. & Davidson, K. W. Emotional triggers in myocardial infarction: do they matter? *Eur. heart J.* **34**, 300–306 (2013).
7. Lampert, R. Emotion and sudden cardiac death. *Expert Rev. Cardiovasc. Ther.* **7**, 723–725 (2009).
8. Sosnowska-Pasiarska, B., Bakowski, D., Woronowicz-Chrosciel, A. & Wozakowska-Kaplon, B. Sudden cardiac arrest in takotsubo cardiomyopathy - a case study. *Postepy Kardiol. Interwencyjnej.* **10**, 110–113 (2014).

9. Steptoe, A. & Kivimaki, M. Stress and cardiovascular disease: an update on current knowledge. *Annu. Rev. Public Health* **34**, 337–354 (2013).

10. Frasure-Smith, N. et al. Social support, depression, and mortality during the first year after myocardial infarction. *Circulation* **101**, 1919–1924 (2000).

11. Atrooz, F., Alkadhi, K. A. & Salim, S. Understanding stress: insights from rodent models. *Curr. Res. Neurobiol.* **2**, 100013–100013 (2021).

12. de Chaves, E. P. & Narayanaswami, V. Apolipoprotein E and cholesterol in aging and disease in the brain. *Future Lipidol.* **3**, 505–530 (2008).

13. Johnson, L. A. et al. Apolipoprotein E-low density lipoprotein receptor interaction affects spatial memory retention and brain ApoE levels in an isoform-dependent manner. *Neurobiol. Dis.* **64**, 150–162 (2014).

14. Wang, Y. X. Cardiovascular functional phenotypes and pharmacological responses in apolipoprotein E deficient mice. *Neurobiol. Aging* **26**, 309–316 (2005).

15. Wang, Y. X. et al. Inhibition of Rho-kinase by fasudil attenuated angiotensin II-induced cardiac hypertrophy in apolipoprotein E deficient mice. *Eur. J. Pharm.* **512**, 215–222 (2005).

16. Pendse, A. A., Arbones-Mainar, J. M., Johnson, L. A., Altenburg, M. K. & Maeda, N. Apolipoprotein E knock-out and knock-in mice: atherosclerosis, metabolic syndrome, and beyond. *J. Lipid Res.* **50**, S178–S182 (2009).

17. Serrano-Pozo, A., Das, S. & Hyman, B. T. APOE and Alzheimer's disease: advances in genetics, pathophysiology, and therapeutic approaches. *Lancet Neurol.* **20**, 68–80 (2021).

18. Xu, M. et al. Apolipoprotein E gene variants and risk of coronary heart disease: a meta-analysis. *Biomed. Res. Int.* **2016**, 3912175 (2016).

19. Liehn, E. A. et al. Apolipoprotein E in cardiovascular diseases: novel aspects of an old-fashioned enigma. *Arch. Med. Res* **49**, 522–529 (2018).

20. Dose, J., Huebbe, P., Nebel, A. & Rimbach, G. APOE genotype and stress response - a mini review. *Lipids Health Dis.* **15**, 121 (2016).

21. Liu, B. R. et al. Apoe-knockout induces strong vascular oxidative stress and significant changes in the gene expression profile related to the pathways implicated in redox, inflammation, and endothelial function. *Cell Signal* **108**, 110696 (2023).

22. Tahrir, F. G., Langford, D., Amini, S., Ahooyi, T. M. & Khalili, K. Mitochondrial quality control in cardiac cells: mechanisms and role in cardiac cell injury and disease. *J. Cell Physiol.* **234**, 8122–8133 (2019).

23. Yin, J. X. et al. Effect of ApoE isoforms on mitochondria in Alzheimer disease. *Neurology* **94**, E2404–E2411 (2020).

24. Schmukler, E. et al. Altered mitochondrial dynamics and function in APOE4-expressing astrocytes. *Cell Death Dis.* **11**, 578 (2020).

25. Rueter, J., Rimbach, G. & Huebbe, P. Functional diversity of apolipoprotein E: from subcellular localization to mitochondrial function. *Cell. Mol. Life Sci.* **79**, 499 (2022).

26. Gabrielli, A. P. et al. Mitochondria profoundly influence apolipoprotein E biology. *J. Alzheimer's Dis.* **92**, 591–604 (2023).

27. Lin, Y. et al. Global profiling of Rbm24 bound RNAs uncovers a multi-tasking RNA binding protein. *Int. J. Biochem. Cell Biol.* **94**, 10–21 (2018).

28. Zhang, M. et al. Rbm24, a target of p53, is necessary for proper expression of p53 and heart development. *Cell Death Differ.* **25**, 1118–1130 (2018).

29. Xu, X. Q. et al. Highly enriched cardiomyocytes from human embryonic stem cells. *Cytotherapy* **10**, 376–389 (2008).

30. Xu, X. Q., Soo, S. Y., Sun, W. & Zweigerdt, R. Global expression profile of highly enriched cardiomyocytes derived from human embryonic stem cells. *Stem Cells* **27**, 2163–2174 (2009).

31. Yang, J. et al. RBM24 is a major regulator of muscle-specific alternative splicing. *Dev. Cell* **31**, 87–99 (2014).

32. Dash, S. et al. The master transcription factor SOX2, mutated in anophthalmia/microphthalmia, is post-transcriptionally regulated by the conserved RNA-binding protein RBM24 in vertebrate eye development. *Hum. Mol. Genet.* **29**, 591–604 (2020).

33. Poon, K. L. et al. RNA-binding protein RBM24 is required for sarcomere assembly and heart contractility. *Cardiovasc. Res.* **94**, 418–427 (2012).

34. Zheng, L. et al. Rbm24 regulates inner-ear-specific alternative splicing and is essential for maintaining auditory and motor coordination. *RNA Biol.* **18**, 468–480 (2021).

35. Liu, J., Kong, X., Zhang, M., Yang, X. & Xu, X. RNA binding protein 24 deletion disrupts global alternative splicing and causes dilated cardiomyopathy. *Protein Cell* **10**, 405–416 (2019).

36. van den Hoogenhof, M. M. G. et al. AAV9-mediated Rbm24 overexpression induces fibrosis in the mouse heart. *Sci. Rep.* **8**, 11696 (2018).

37. Liu, J. et al. RBM24 controls cardiac QT interval through CaMKII delta splicing. *Cell Mol. Life Sci.* **79**, 613 (2022).

38. Zhang, J. et al. The RNA-binding protein RBM24 regulates lipid metabolism and SLC7A11 mRNA stability to modulate ferroptosis and inflammatory response. *Front. Cell Dev. Biol.* **10**, 1008576 (2022). doi:ARTN.

39. Zhang, M., Zhang, J., Chen, X., Cho, S. J. & Chen, X. Glycogen synthase kinase 3 promotes p53 mRNA translation via phosphorylation of RNPC1. *Genes Dev.* **27**, 2246–2258 (2013).

40. Sun, L. et al. Mammalian eIF4E2-GSK3beta maintains basal phosphorylation of p53 to resist senescence under hypoxia. *Cell Death Dis.* **13**, 459 (2022).

41. Sun, W. et al. Fine-tuning p53 activity by modulating the interaction between eukaryotic translation initiation factor eIF4E and RNA-binding protein RBM38. *Genes Dev.* **35**, 542–555 (2021).

42. Wang, Y., Li, W., Zhang, C., Peng, W. & Xu, Z. RBM24 is localized to stress granules in cells under various stress conditions. *Biochem. Biophys. Res. Commun.* **608**, 96–101 (2022).

43. Rosen, J. B., Asok, A. & Chakraborty, T. The smell of fear: innate threat of 2,5-dihydro-2,4,5-trimethylthiazoline, a single molecule component of a predator odor. *Front. Neurosci.* **9**, 292 (2015).

44. Mair, J. et al. How is cardiac troponin released from injured myocardium? *Eur. heart J. Acute Cardiovasc. Care* **7**, 553–560 (2018).

45. Lucchesi, C. A., Zhang, J., Ma, B., Chen, M. & Chen, X. Disruption of the Rbm38-eIF4E complex with a synthetic peptide Pep8 increases p53 expression. *Cancer Res.* **79**, 807–818 (2019).

46. Liu, S., Liu, J., Weng, R., Gu, X. & Zhong, Z. Apolipoprotein E gene polymorphism and the risk of cardiovascular disease and type 2 diabetes. *BMC Cardiovasc. Disord.* **19**, 213 (2019).

47. Andres, A. M. et al. Mitophagy is required for acute cardioprotection by simvastatin. *Antioxid. Redox Signal.* **21**, 1960–1973 (2014).

48. Miller, L., Bodemeier Loayza Careaga, M., Handa, R. J. & Wu, T. J. The effects of chronic variable stress and photoperiod alteration on the hypothalamic-pituitary-adrenal axis response and behavior of mice. *Neuroscience* **496**, 105–118 (2022).

49. Deng, Y. Q. et al. Rab18 binds PLIN2 and ACSL3 to mediate lipid droplet dynamics. *Biochem. Biophys. Acta Mol. Cell Biol. Lipids* **1866**, 158923 (2021).

50. Burton, F. L. & Cobbe, S. M. Dispersion of ventricular repolarization and refractory period. *Cardiovasc. Res.* **50**, 10–23 (2001).

51. Hou, T. T. et al. NDUFAB1 confers cardio-protection by enhancing mitochondrial bioenergetics through coordination of respiratory complex and supercomplex assembly. *Cell Res.* **29**, 754–766 (2019).

52. Shin, M. et al. Targeting protein and peptide therapeutics to the heart via tannic acid modification. *Nat. Biomed. Eng.* **2**, 304–317 (2018).

53. Stambolic, V., Ruel, L. & Woodgett, J. R. Lithium inhibits glycogen synthase kinase-3 activity and mimics wingless signalling in intact cells. *Curr. Biol.* **6**, 1664–1668 (1996).

54. Rogerson, D. T. et al. Efficient genetic encoding of phosphoserine and its nonhydrolyzable analog. *Nat. Chem. Biol.* **11**, 496–49 (2015).

55. Freak-Poli, R., Phyo, A. Z. Z., Hu, J. & Barker, S. F. Are social isolation, lack of social support or loneliness risk factors for cardiovascular disease in Australia and New Zealand? A systematic review and meta-analysis. *Health Promot. J. Austr* **33**, 278–315 (2022).

56. Tomova, L. et al. Acute social isolation evokes midbrain craving responses similar to hunger. *Nat. Neurosci.* **23**, 1597–1605 (2020).

57. Rozanski, A., Blumenthal, J. A. & Kaplan, J. Impact of psychological factors on the pathogenesis of cardiovascular disease and implications for therapy. *Circulation* **99**, 2192–2217 (1999).

58. Harris, K. M., Jacoby, D. L., Lampert, R., Soucier, R. J. & Burg, M. M. Psychological stress in heart failure: a potentially actionable disease modifier. *Heart Fail. Rev.* **26**, 561–575 (2021).

59. Endrighi, R. et al. Psychological stress and short-term hospitalisations or death in patients with heart failure. *Heart* **102**, 1820–1825 (2016).

60. Henein, M. Y., Vancheri, S., Longo, G. & Vancheri, F. The impact of mental stress on cardiovascular health-part II. *J. Clin. Med.* https://doi.org/10.3390/jcm11154405 (2022).

61. Kim, E. S., Smith, J. & Kubzansky, L. D. Prospective study of the association between dispositional optimism and incident heart failure. *Circ. Heart Fail.* **7**, 394–400 (2014).

62. Pelliccia, F., Kaski, J. C., Crea, F. & Camici, P. G. Pathophysiology of Takotsubo syndrome. *Circulation* **135**, 2426–2441 (2017).

63. Mendez-Giraldez, R. et al. GWAS of the electrocardiographic QT interval in Hispanics/Latinos generalizes previously identified loci and identifies population-specific signals. *Sci. Rep.* **7**, 17075 (2017).

64. Nakajima, T., Kaneko, Y. & Kurabayashi, M. Unveiling specific triggers and precipitating factors for fatal cardiac events in inherited arrhythmia syndromes. *Circ. J.* **79**, 1185–1192 (2015).

65. Agrimi, J. et al. Psychosocial stress hastens disease progression and sudden death in mice with arrhythmogenic cardiomyopathy. *J. Clin. Med.* **9**, 3804 (2020). doi:ARTN.

66. Lampert, R. Anger and ventricular arrhythmias. *Curr. Opin. Cardiol.* **25**, 46–52 (2010).

67. Shusterman, V. & Lampert, R. Role of stress in cardiac arrhythmias. *J. Atr. Fibrillation* **5**, 834 (2013).

68. Levy, S. et al. Characterization of different subsets of atrial fibrillation in general practice in France: the ALFA study. The College of French Cardiologists. *Circulation* **99**, 3028–3035 (1999).

69. Lampert, R. et al. Triggering of symptomatic atrial fibrillation by negative emotion. *J. Am. Coll. Cardiol.* **64**, 1533–1534 (2014).

70. Thompson, T. S. et al. The effect of anxiety and depression on symptoms attributed to atrial fibrillation. *Pacing Clin. Electrophysiol.* **37**, 439–446 (2014).

71. Ladwig, K. H., Goette, A., Atasoy, S. & Johar, H. Psychological aspects of atrial fibrillation: a systematic narrative review: impact on incidence, cognition, prognosis, and symptom perception. *Curr. Cardiol. Rep.* **22**, 137 (2020).

72. Wu, J. H., Hagaman, J., Kim, S., Reddick, R. L. & Maeda, N. Aortic constriction exacerbates atherosclerosis and induces cardiac dysfunction in mice lacking apolipoprotein E. *Arterioscler. Thromb. Vasc. Biol.* **22**, 469–475 (2002).

73. Qin, Y. W. et al. Simvastatin inhibited cardiac hypertrophy and fibrosis in apolipoprotein E-deficient mice fed a "Western-style diet" by increasing PPAR alpha and gamma expression and reducing TC, MMP-9, and Cat S levels. *Acta Pharmacol. Sin.* **31**, 1350–1358 (2010).

74. Gonzalez, A., Schelbert, E. B., Diez, J. & Butler, J. Myocardial interstitial fibrosis in heart failure: biological and translational perspectives. *J. Am. Coll. Cardiol.* **71**, 1696–1706 (2018).

75. Bayer, J. D. et al. Acetylcholine delays atrial activation to facilitate atrial fibrillation. *Front. Physiol.* **10**, 1105 (2019).

76. Xie, W. J. et al. Mitochondrial oxidative stress promotes atrial fibrillation. *Sci. Rep.* **5**, 11427 (2015).

77. Karam, B. S., Chavez-Moreno, A., Koh, W., Akar, J. G. & Akar, F. G. Oxidative stress and inflammation as central mediators of atrial fibrillation in obesity and diabetes. *Cardiovasc. Diabetol.* **16**, 120 (2017).

78. Mason, F. E., Pronto, J. R. D., Alhussini, K., Maack, C. & Voigt, N. Cellular and mitochondrial mechanisms of atrial fibrillation. *Basic Res. Cardiol.* **115**, 72 (2020).

79. Peoples, J. N., Saraf, A., Ghazal, N., Pham, T. T. & Kwong, J. Q. Mitochondrial dysfunction and oxidative stress in heart disease. *Exp. Mol. Med.* **51**, 162 (2019).

80. Cynthia Rocha, C. S.-B., Whitesell, T. & Bergdahl, A. Implications of apolipoprotein E deficiencyon cardiac mitochondrial oxygen consumption in a young mouse model. *Eur. J. Cardiovasc. Med.* **III**, 394–400 (2014).

81. Rocha, C., Koury, O. H., Scheede-Bergdahl, C. & Bergdahl, A. Cardiac mitochondrial respiration following a low-carbohydrate, high-fat diet in apolipoprotein E-deficient mice. *J. Physiol. Biochem.* **75**, 65–72 (2019).

82. Chen, W. Y. et al. Role of apolipoprotein E in electronegative low-density lipoprotein-induced mitochondrial dysfunction in cardiomyocytes. *Metabolism* **107**, 154227 (2020).

83. Bharti, V., Bhardwaj, A., Elias, D. A., Metcalfe, A. W. S. & Kim, J. S. A systematic review and meta-analysis of lipid signatures in post-traumatic stress disorder. *Front. Psychiatry* **13**, 847310 (2022).

84. Bharti, V. et al. A systematic review and meta-analysis of lipid metabolomic signatures of major depressive disorder. *J. Psychiatr. Res.* **139**, 197–205 (2021).

85. Agrimi, J. et al. Obese mice exposed to psychosocial stress display cardiac and hippocampal dysfunction associated with local brain-derived neurotrophic factor depletion. *Ebiomedicine* **47**, 384–401 (2019).

86. Shizukuda, Y., Matoba, S., Mian, O. Y., Nguyen, T. & Hwang, P. M. Targeted disruption of p53 attenuates doxorubicin-induced cardiac toxicity in mice. *Mol. Cell Biochem.* **273**, 25–32 (2005).

87. Gogiraju, R. et al. Endothelial p53 deletion improves angiogenesis and prevents cardiac fibrosis and heart failure induced by pressure overload in mice. *J. Am. Heart Assoc.* https://doi.org/10.1161/JAHA.115.001770 (2015).

88. Guevara, N. V., Kim, H. S., Antonova, E. I. & Chan, L. The absence of p53 accelerates atherosclerosis by increasing cell proliferation. *Nat. Med.* **5**, 335–339 (1999).

89. Kamenska, A., Simpson, C. & Standart, N. eIF4E-binding proteins: new factors, new locations, new roles. *Biochem. Soc. Trans.* **42**, 1238–1245 (2014).

90. Tomova, L. et al. Acute social isolation evokes midbrain craving responses similar to hunger. *Nat. Neurosci.* **25**, 399–399 (2022).

91. Machida, M. et al. Purification of phosphoproteins by immobilized metal affinity chromatography and its application to phosphoproteome analysis. *FEBS J.* **274**, 1576–1587 (2007).

92. Jaros, J. A. et al. Clinical use of phosphorylated proteins in blood serum analysed by immobilised metal ion affinity chromatography and mass spectrometry. *J. Proteom.* **76**, 36–42 (2012).

93. Rogerson, D. T. et al. Efficient genetic encoding of phosphoserine and its nonhydrolyzable analog. *Nat. Chem. Biol.* **11**, 496–503 (2015).

94. Zhang, X. Q. et al. Mutation in nuclear pore component NUP155 leads to atrial fibrillation and early sudden cardiac death. *Cell* **135**, 1017–1027 (2008).

95. Zhang, X. et al. Mutation in nuclear pore component NUP155 leads to atrial fibrillation and early sudden cardiac death. *Cell* **135**, 1017–1027 (2008).

## Acknowledgements

## Author contributions

Statement M.Z. and Q.K.W. conceived and designed the study. H.Y. and L.S. performed most experiments. X.B., H.L., B.C., C.F., X.Z., C.Z., D.L., and Y.Y. performed electrocardiograms, echocardiography, and cardiomyocyte action potential. Z.T., B.D., Y.B., L.L., X.H., B.L., and Y.Y. helped experiments such as RNC-Seq and behavioral experiments in mice. Z.H. and G.S. helped with experiments on human social isolation. Z.D. and S.L. helped revise the manuscript. M.Z. and Q.K.W. supervised the project and analyzed the data; M.Z., Q.K.W., H.Y., and L.S. wrote the manuscript. All authors read and commented on the draft version of the manuscript and approved the final version.

## Competing interests

The authors declare no competing interests.

## Additional information

**Supplementary information** The online version contains supplementary material available at https://doi.org/10.1038/s41467-024-54519-0.

**Correspondence** and requests for materials should be addressed to Hui Li, Qing K. Wang or Min Zhang.

**Peer review information** *Nature Communications* thanks Nazareno Paolocci, Mirko Völkers, and the other, anonymous, reviewers for their contribution to the peer review of this work. A peer review file is available.

**Reprints and permissions information** is available at http://www.nature.com/reprints

**Publisher's note** Springer Nature remains neutral with regard to jurisdictional claims in published maps and institutional affiliations.